

# Quantum-circuit guide to optical and atomic interferometry

Carlton M. Caves<sup>1,\*</sup> and Anil Shaji<sup>2,†</sup>

<sup>1</sup>*Center for Quantum Information and Control,  
University of New Mexico, Albuquerque, New Mexico 87131-0001, USA*

<sup>2</sup>*Indian Institute of Science Education and Research,  
Thiruvananthapuram, Kerala 695016, India*

Atomic (qubit) and optical or microwave (modal) phase-estimation protocols are placed on the same footing in terms of quantum-circuit diagrams. Circuit equivalences are used to demonstrate the equivalence of protocols that achieve the Heisenberg limit by employing entangled superpositions of Fock states, such as N00N states. The key equivalences are those that disentangle a circuit so that phase information is written exclusively on a mode or modes or on a qubit. The Fock-state-superposition phase-estimation circuits are converted to use entangled coherent-state superpositions; the resulting protocols are more amenable to realization in the lab, particularly in a qubit/cavity setting at microwave frequencies.

PACS numbers: 42.50.St, 06.20.-f, 07.60.Ly, 35.25.+k

Keywords: interferometry, phase estimation, quantum circuits, disentanglement

## I. INTRODUCTION

Atomic and optical (or microwave) interferometers are standard tools for high-precision metrology: the quantity to be measured is mapped onto the phases of internal levels of atoms or the paths or polarizations of photons, and the phase is estimated by interferometry. The conventional way of operating an interferometer, using independent (unentangled) atoms or independent (unentangled) photons, i.e., photons created and processed by the techniques of linear optics alone, has a sensitivity limit that scales as  $1/\sqrt{N}$ , where  $N$  is the number of atoms or photons devoted to the task. This scaling is called the *quantum noise limit* or the *shot-noise limit* [1].

The sensitivity of an interferometer can be improved by entangling the atoms or photons. The ultimate sensitivity is obtained by using so-called cat states in atomic interferometry [2, 3, 4] or their analogue, N00N states, in optical interferometry [5, 6, 7, 8, 9, 10, 11, 12]. The moniker N00N, which comes from the (unnormalized) form,  $|N, 0\rangle + |0, N\rangle$ , was applied and popularized by Dowling and collaborators [8, 12]. The use of entanglement permits a sensitivity that scales as  $1/N$ , a scaling often called the *Heisenberg limit* [13, 14, 15]. There are many closely related ideas for achieving Heisenberg-limited scaling, some of which don't look like an interferometer at all (because they aren't) and don't require any entanglement. In this paper we use the pictorial representation of quantum-circuit diagrams to put atomic and optical interferometry on the same footing and to demonstrate the equivalence of various methods for achieving the Heisenberg limit.

In its translations from atoms to photons, this paper formulates a quantum-circuit version of the equivalence between atomic and optical interferometry demonstrated by Yurke, McCall, and Klauder [16]. Much of the paper's content on phase estimation and interferometry is anticipated by the work of Gerry and collaborators [5, 7, 9, 10, 17], and many of the qubit-mode operations discussed in the paper follow a path blazed by Davidovich, Haroche, and collaborators [18, 19, 20, 21, 22, 23, 24]. Lee, Kok, and Dowling [8] made an initial foray into the domain of quantum circuits as tools for investigating equivalent atomic and optical interferometers, calling this the "quantum

---

\*Electronic address: caves@info.phys.unm.edu

†Electronic address: shaji@iisertvm.ac.in

Rosetta stone.” Less lofty, but more ambitious, this article aims to establish a permanent beachhead on this terrain, making it a standard tool for analyzing interferometers and phase estimation.

This article is dedicated to the memory of Krzysztof Wódkiewicz. When new ideas came along, as in the quantum-information revolution, Krzysztof embraced them and incorporated them into his suite of theoretical tools. Indeed, this contribution is very much in the spirit of his own recent work on qubit decoherence [25, 26, 27, 28, 29], something he knew as well as anyone, but which he rethought, reëxamined, and reformulated in the light of the modern language of quantum operations and Kraus operators. In the same way, this contribution repackages concepts from optical and atomic interferometry, concepts that all physicists know, but presented here from a different perspective. It is to be hoped that the paper lives up to Krzysztof’s high standards. The paper also represents an experiment that CMC has long wanted to try: writing a paper in which the figures and captions outweigh the text.

Section II describes atomic interferometry in terms of qubits and optical interferometry in terms of modes, reviewing how to map the states and unitary operations for qubits to those for modes; it introduces the language of quantum circuits, with particular attention to how measurements are represented and manipulated within the quantum-circuit picture and the role of disentanglement in interferometry. Section III reviews the description of conventional, quantum-noise-limited interferometers in terms of circuit diagrams. Section IV turns to Heisenberg-limited modal interferometers. It considers phase-estimation protocols that are best thought of as using superpositions of Fock states, and Sec. V discusses the analogous protocols that use superpositions of coherent states. A concluding Sec. VI briefly considers how Heisenberg-limited phase estimation might be implemented in the lab and then wraps up with a peroration to circuit diagrams as the best way to represent general protocols for phase estimation and interferometry.

## II. QUBITS AND MODES

### A. States, gates, and quantum circuits

Atomic interferometry deals with atoms, idealized as having two levels. Any such two-level system can be regarded as a qubit, which has two standard states, a “ground” state  $|1\rangle$  and an “excited” state  $|0\rangle$ . Thus we often refer to atomic interferometry as qubit interferometry.

The pure states of a qubit are conveniently thought of as lying on a Bloch sphere defined by Pauli operators  $Z = \sigma_z = |0\rangle\langle 0| - |1\rangle\langle 1|$ ,  $X = \sigma_x = |0\rangle\langle 1| + |1\rangle\langle 0|$ , and  $Y = \sigma_y = -i(|0\rangle\langle 1| - |1\rangle\langle 0|)$ . We use Latin letters at the beginning of the alphabet to represent bit values, 0 and 1, and we use Latin letters at the end of the alphabet to denote the sign representation of a bit value, e.g.,  $Z|a\rangle = (-1)^a|a\rangle = z|a\rangle$ . When we have  $N$  qubits, we introduce a total “angular momentum” operator  $\mathbf{J} = \frac{1}{2} \sum_{j=1}^N \boldsymbol{\sigma}_j$ . We denote the product basis of standard states by  $|\mathbf{a}\rangle = |a_1\rangle \otimes \cdots \otimes |a_N\rangle$ , where  $\mathbf{a}$  stands for the bit string  $a_1 \dots a_N$ . For qubit interferometry, we are interested in symmetric qubit states. The  $(N + 1)$ -dimensional symmetric subspace is spanned by the states

$$|n_0, n_1\rangle = |J = N/2, m = (n_0 - n_1)/2\rangle = \sqrt{\frac{n_0!n_1!}{N!}} \sum_{\mathbf{a}} |\mathbf{a}\rangle, \quad (2.1)$$

where  $n_0$  is the number of atoms in state  $|0\rangle$  and  $n_1$  is the number in state  $|1\rangle$ , and where the sum runs over all strings  $\mathbf{a}$  that have  $n_0$  0s and  $n_1$  1s.

In optical or microwave interferometry we deal with two modes of the electromagnetic field, labeled 0 and 1, with annihilation operators  $a$  and  $b$ . Thus we often refer to optical interferometry as modal interferometry. The number operators for the two modes are denoted  $N_0 = a^\dagger a$  and

$N_1 = b^\dagger b$ . The Fock basis of photon-number eigenstates for the two modes is defined by

$$|n_0, n_1\rangle_\sim = \frac{(a^\dagger)^{n_0}}{\sqrt{n_0!}} \frac{(b^\dagger)^{n_1}}{\sqrt{n_1!}} |0, 0\rangle_\sim, \quad (2.2)$$

where  $|0, 0\rangle_\sim$  is the vacuum state of the two modes, and where  $n_0$  is the number of photons in mode 0 and  $n_1$  the number in mode 1. The connection to qubit interferometry is made by identifying these Fock states with the symmetric qubit states denoted in the same way. The squiggle in Eq. (2.2) is the symbol we use for modes; we almost always omit it in state designations. For  $N = 1$ , the Fock states are the dual-rail logical states of linear-optical quantum computing [30, 31],  $|1, 0\rangle_\sim = |0\rangle$  and  $|0, 1\rangle_\sim = |1\rangle$ . For  $N = 2$ , the Fock states are  $|2, 0\rangle_\sim = |00\rangle$ ,  $|1, 1\rangle_\sim = (|01\rangle + |10\rangle)/\sqrt{2}$ , and  $|0, 2\rangle_\sim = |11\rangle$ .

The identification of symmetric qubits with modes is completed by introducing the angular-momentum operators of the Schwinger representation:

$$J_z = \frac{1}{2}(a^\dagger a - b^\dagger b) = \frac{1}{2} \sum_{j=1}^N Z_j, \quad (2.3a)$$

$$J_x = \frac{1}{2}(a^\dagger b + b^\dagger a) = \frac{1}{2} \sum_{j=1}^N X_j, \quad (2.3b)$$

$$J_y = -\frac{i}{2}(a^\dagger b - b^\dagger a) = \frac{1}{2} \sum_{j=1}^N Y_j. \quad (2.3c)$$

The photon-number operator is  $N = a^\dagger a + b^\dagger b$ . The identification of the  $N$ -photon subspace of the two modes with the symmetric subspace of  $N$  qubits is the foundation for unifying optical and atomic interferometry. Of course, when dealing with modes, we can also have superpositions of different total photon numbers. These superposition states do not have a convenient representation in terms of qubits, but we will be able to represent them in our circuit diagrams.

The allowed unitary operations, or gates, are symmetric unitary operators on the  $N$  qubits or, equivalently, photon-number preserving unitaries for the two modes. All such unitaries, up to a global  $N$ -dependent phase, can be written as  $e^{-if(\mathbf{J})}$ , where  $f(\mathbf{J})$  is a Hermitian function of the total angular momentum [32].

An important special case occurs when  $f$  is linear, in which case the unitaries, rotations  $e^{-i\mathbf{J}\cdot\hat{\mathbf{n}}\theta} = (e^{-i\boldsymbol{\sigma}\cdot\hat{\mathbf{n}}\theta/2})^{\otimes N}$  in the angular-momentum sense, are independent, identical unitaries on the qubits or, equivalently, the operations of linear optics on the two modes. The operation of such a unitary is summarized by how it transforms the modal creation operators:

$$e^{-i\mathbf{J}\cdot\hat{\mathbf{n}}\theta} \begin{pmatrix} a^\dagger \\ b^\dagger \end{pmatrix} e^{i\mathbf{J}\cdot\hat{\mathbf{n}}\theta} = M^T \begin{pmatrix} a^\dagger \\ b^\dagger \end{pmatrix}. \quad (2.4)$$

Here  $M$  is a  $2 \times 2$  unitary matrix independent of  $N$ , and  $T$  denotes the transpose. Applying both sides of Eq. (2.4) to the modal vacuum state and converting to qubit notation gives

$$e^{-i\boldsymbol{\sigma}\cdot\hat{\mathbf{n}}\theta/2} \begin{pmatrix} |0\rangle \\ |1\rangle \end{pmatrix} = M^T \begin{pmatrix} |0\rangle \\ |1\rangle \end{pmatrix}, \quad (2.5)$$

from which it follows that  $M$  is the representation of  $e^{-i\boldsymbol{\sigma}\cdot\hat{\mathbf{n}}\theta/2}$  in the standard qubit basis, i.e.,  $M_{ab} = \langle a | e^{-i\boldsymbol{\sigma}\cdot\hat{\mathbf{n}}\theta/2} | b \rangle$ . The matrix  $M$  is given explicitly by

$$M = \begin{pmatrix} \cos(\theta/2) - in_z \sin(\theta/2) & (-in_x - n_y) \sin(\theta/2) \\ (-in_x + n_y) \sin(\theta/2) & \cos(\theta/2) + in_z \sin(\theta/2) \end{pmatrix}. \quad (2.6)$$

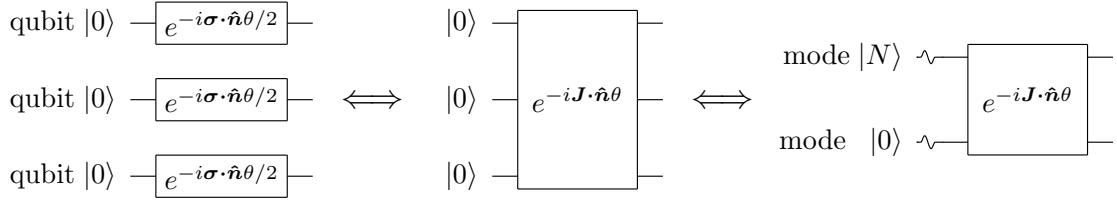


FIG. 1: Linear-optical quantum gate in qubit form on the left, in terms of Schwinger operators for qubits in the middle, and in modal form on the right. The qubits provide a particle description, and the modes provide a wave description: the qubits are the particles—say, atoms or photons—that occupy the modes 0 and 1, and the modes are the single-particle states,  $|0\rangle$  and  $|1\rangle$ , of the qubits. In qubit circuits we use  $N = 3$  qubits for illustration (occasionally  $N = 5$ ), here and in the following, but the equivalences to modal circuits are valid for arbitrary  $N$ . A state to the left of a circuit wire indicates the input to that wire; if no state is given, equivalences are independent of the input state, as they would be here. Equivalences between qubit and modal circuits require, however, that the input state be in the symmetric subspace of  $N$  qubits or, equivalently, in the  $N$ -photon sector for modes. On the left and right, wires are labeled explicitly by whether they are qubits or modes; hereafter, we omit this labeling and use a squiggle, as in the right circuit, to designate a modal wire. When  $\hat{n}$  lies in the equatorial plane, these are, for  $\theta = \pi/2$ ,  $\pi/2$  transitions for qubits and 50/50 beamsplitters for modes and, for  $\theta = \pi$ , qubit FLIP operators and modal SWAP operators.

Suppose  $\hat{n} = \hat{x} \cos \phi + \hat{y} \sin \phi$  lies in the equatorial plane. If  $\theta = \pi/2$ , these are  $\pi/2$  transitions for qubits and 50/50 beamsplitters for modes, with transformation matrix (2.6) given by

$$M = \frac{1}{\sqrt{2}} \begin{pmatrix} 1 & -ie^{-i\phi} \\ -ie^{i\phi} & 1 \end{pmatrix}. \quad (2.7)$$

If  $\theta = \pi$ , these are qubit FLIP gates and modal SWAP gates, with additional phase shifts; i.e.,  $e^{-iJ \cdot \hat{n}\pi} = (-i\sigma \cdot \hat{n})^{\otimes N}$  has transformation matrix

$$M = \begin{pmatrix} 0 & -ie^{-i\phi} \\ -ie^{i\phi} & 0 \end{pmatrix}. \quad (2.8)$$

Notice also that  $Z^{\otimes N} = i^N e^{-iJ_z\pi} = e^{ib^\dagger b\pi} = I \otimes \Pi$ , with  $\Pi$  being the modal parity operator, and that  $(-Z)^{\otimes N} = (-i)^N e^{-iJ_z\pi} = e^{-ia^\dagger a\pi} = \Pi \otimes I$ . A  $2\pi$  rotation about any axis  $\hat{n}$  has  $M = I$  and  $e^{-iJ \cdot \hat{n}2\pi} = (-1)^N = \Pi \otimes \Pi$ .

These considerations provide an opportunity to introduce quantum circuits in Figs. 1 and 2. We use generally conventional circuit notation [33], with wires representing qubits or modes and unitary gates enclosed in rectangular boxes, but we use an initial squiggle to indicate when a wire applies to a mode. We make frequent use of the qubit Hadamard and  $S$  gates:

$$H \equiv ie^{-i[(X+Z)/\sqrt{2}]\pi/2} = \frac{1}{\sqrt{2}}(X + Z) \quad \Leftrightarrow \quad \frac{1}{\sqrt{2}} \begin{pmatrix} 1 & 1 \\ 1 & -1 \end{pmatrix}, \quad (2.9)$$

$$S \equiv e^{i\pi/4} e^{-iZ\pi/4} \quad \Leftrightarrow \quad \begin{pmatrix} 1 & 0 \\ 0 & i \end{pmatrix}. \quad (2.10)$$

Notice that  $e^{-iY\pi/4} = (I - iY)/\sqrt{2} = XH = HZ$ . Controlled application of a unitary is represented conventionally by a circle on the control qubit connected by a line to the unitary on the target. Control on  $|1\rangle$  is represented by a filled circle, and control on  $|0\rangle$  by an open circle. Figure 1 is the circuit form of the equivalence between qubit and modal gates for linear-optical transformations.



in (b), which for qubits differ from those in (a) only by a set of local gates, entangle both qubits and modes; the gates in (c) are products for qubits and for modes.

We emphasize that qubit and two-mode interferometers can always be thought of in both ways, as involving particles or modes—that’s the complementarity of quantum mechanics—but we prefer to think one way or the other, perhaps to our detriment. We generally like to regard atomic interferometry as using particles and optical or microwave interferometry as using modes, but the other way of thinking is available in both cases. There is one situation, atomic interferometry using a two-component Bose-Einstein condensate (BEC), where it is so natural to think in both ways that it is especially valuable to be able to translate between the two ways of thinking.

## B. Measurements and circuit equivalences

The remaining ingredient needed in our circuit diagrams is a representation of measurements. For qubits, we are interested in symmetric measurements and thus can specialize to measurements of a particular Pauli component  $\sigma \cdot \hat{n}$ , usually  $Z$ , on all qubits. We write the  $\pm 1$  outcome of a measurement of a Pauli component as  $z = (-1)^a$ . Most discussions of qubit measurements regard the bit value  $a$  as the outcome, but in this paper we always think of  $z$  as the outcome. For modes, the only measurement we need is the measurement that counts photons in a mode.

In our circuit diagrams, measurements are represented by bubbles (rounded boxes), with the measured observable inside the bubble. For photon counting, we adopt a special notation, illustrated in Fig. 3, in which the measurement is represented by the conventional symbol for a photodetector. We are only interested in the outcome of a measurement and its statistics and not in the post-measurement state of the measured system; in the lingo of quantum measurement theory, this means we are interested in the measurement’s POVM, but not in the quantum operation that outputs a post-measurement state. Thus, in our circuits, there is no quantum wire emerging from a measurement bubble; the only output from a bubble is a double (classical) wire that carries the value of the outcome. The values on such classical wires can be manipulated by classical gates, which we depict as rectangular boxes. We often label a classical wire with the value it carries.

Figure 4 illustrates our measurement notation in the context of two ways of processing the data from  $Z$  measurements on all qubits and the equivalent measurements on modes. The important conclusions are that summing the outcomes of  $Z$  measurements is equivalent to counting photons on the two modes and then differencing the counts, whereas multiplying the outcomes of  $Z$  measurements, i.e., measuring  $Z^{\otimes N}$ , is equivalent to measuring the parity of mode 1 [5, 7, 9].

We need several additional rules for handling measurements, the first three of which, notation for a measurement whose outcome is discarded, the rule for unitarily transforming measured observables, and the principle of deferred measurement [33, 37], are introduced and described in Fig. 5. Figure 6 combines the equivalences of Fig. 5 to derive a new set of equivalences, spelled out in Fig. 6(b), which lie at the heart of interferometry. These equivalences express a very important concept, *disentanglement*, in several different ways. If there is a most important figure to master before considering Heisenberg-limited interferometers, Fig. 6 is it. In using the equivalences of Fig. 6(b), it is important to remember that they require that the unitary operator  $U$  be Hermitian, which means that it is an observable all of whose eigenvalues are equal to  $\pm 1$ , and that for the last two circuits, the  $\pm 1$  eigenspaces of  $U$  have the same dimension.

The equivalence of Fig. 6(a) is also used in Fig. 6(c) to derive a standard method for measuring a Hermitian  $U$ , of which the parity of a field mode is an outstanding example. This measurement is founded on a technique called *phase kickback* [33, 38], which maps the phase of  $U$ ,  $\pm 1$  in this case, to a qubit. Phase kickback is a key element in many quantum algorithms. This qubit-assisted method for measuring the parity of a mode was proposed by Lutterbach and Davidovich [21, 22]

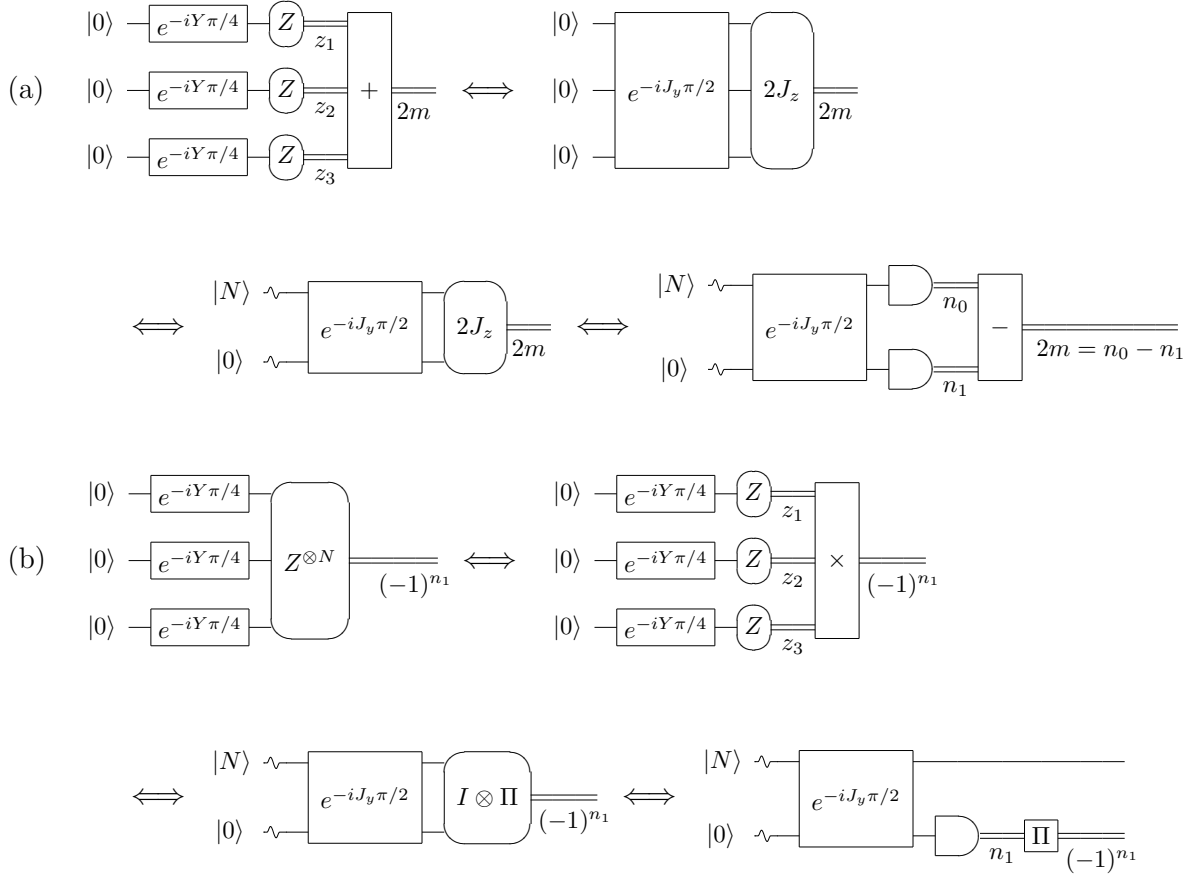


FIG. 4: (a) Measurement of  $Z$  on  $N = 3$  qubits, all of which are prepared in the state  $(|0\rangle + |1\rangle)/\sqrt{2}$ , followed by classical processing that outputs the *sum* of the  $N$  outcomes. The final outcome  $2m = n_0 - n_1$  is the difference between the numbers of qubits found in  $|0\rangle$  and  $|1\rangle$ ; it is distributed binomially, with mean zero and variance  $N$ . The second and third circuits transform from qubits to modes via the Schwinger operators, with the third circuit having  $N$  photons in mode 0 processed through a 50/50 beamsplitter and then subjected to a measurement of the photon-difference operator  $2J_z = N_0 - N_1$ . In the final circuit, the differenced photocounting is achieved by photocounting on each mode, followed by differencing the counts to give outcome  $2m = n_0 - n_1$ . (b) Measurement of  $Z^{\otimes N}$  on  $N = 3$  qubits prepared as in (a), with outcome  $(-1)^{n_1}$  equally likely to be  $\pm 1$ , is equivalent to measuring  $Z$  on all qubits, followed by classical processing that outputs the *product* of the  $N$  outcomes. This measurement is equivalent to measuring the parity  $\Pi = (-1)^{b^{\dagger}b}$  of mode 1. In the final circuit, the parity measurement is achieved by photocounting followed by classical extraction of the parity. Since mode 0 is unmeasured, it can be restored as a quantum wire in the final circuit even though this is not equivalent, strictly speaking, to the third circuit. The quoted probabilities for the outcomes depend on the initial state shown, but the circuit equivalences themselves are independent of initial state.

and implemented in Refs. [39, 40].

The equivalences in Fig. 6(b), though easy to derive from circuit equivalences, have wandered far enough down the road of circuit diagrams that it is instructive to check that we have not gone astray. A good way to do this is to demonstrate the equivalences in the conventional language of state vectors. Suppose that in Fig. 6(b), the input state has the relative-state decomposition

$$|\psi\rangle = \sqrt{q_0}|\psi_0\rangle \otimes |0\rangle + \sqrt{q_1}|\psi_1\rangle \otimes |1\rangle, \quad (2.11)$$

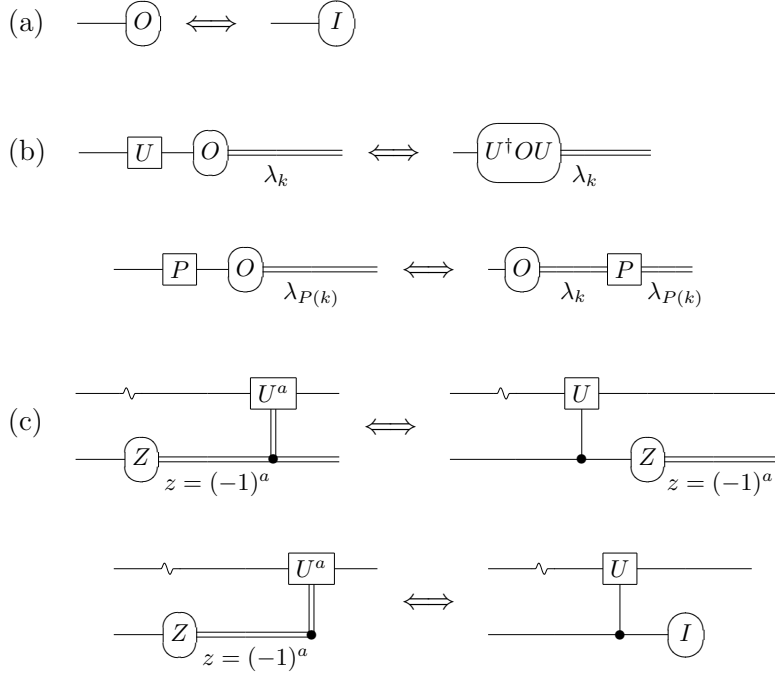


FIG. 5: (a) Measurement of an observable  $O$ , whose outcome is discarded, is represented by a bubble without a classical wire emerging from it. Discarding the outcome implies averaging over the possible outcomes; this is equivalent to tracing out the measured system. We can always represent this as a no-outcome measurement, i.e., a measurement of the unit operator  $I$ ; since a measurement of  $I$  is really no measurement at all—it merely instructs us to trace out that system—we can choose to restore the system to the circuit by eliminating the measurement of  $I$  and extending the quantum wire, *provided we remember that the wire must ultimately be terminated by a measurement without interacting with other wires in the circuit*. (b) Top equivalence: Rule for unitarily transforming a measured observable. Preceding a measurement of observable  $O = \sum_k \lambda_k |k\rangle\langle k|$  with unitary  $U$  is equivalent to measuring the conjugated observable  $U^\dagger O U = \sum_k \lambda_k U^\dagger |k\rangle\langle k| U$ ; in both cases, incoming state  $\sum_k c_k U^\dagger |k\rangle$  yields outcome  $\lambda_k$  with probability  $|c_k|^2$ . Bottom equivalence: Special case in which  $P$  is a unitary that permutes the eigenstates of  $O$ , i.e.,  $P|k\rangle = |P(k)\rangle$ , where  $P(k)$  is a permutation of the indices. In this situation,  $P^\dagger O P = \sum_k \lambda_k |P^{-1}(k)\rangle\langle P^{-1}(k)| = \sum_k \lambda_{P(k)} |k\rangle\langle k|$ ; thus a measurement of  $P^\dagger O P$  is the same as measuring  $O$  and then applying the permutation to the outcome. On both sides of the equivalence, incoming state  $\sum_k c_k |k\rangle$  yields outcome  $\lambda_{P(k)}$  with probability  $|c_k|^2$ . (c) Top equivalence: Principle of deferred measurement, depicted here for a mode and a qubit. Measuring  $Z$  on the qubit and using the outcome to control classically the application of a unitary  $U$  to the mode is the same as applying a controlled- $U$ , with the qubit as control and the mode as target, and then measuring  $Z$  on the qubit. In the latter case, the control is done coherently, and the outcome of the measurement later reveals whether the unitary was applied. Bottom equivalence: Same principle, but with the outcome of the  $Z$  measurement discarded after application of the classical control.

where the states  $|\psi_0\rangle$  and  $|\psi_1\rangle$ , though normalized, are not necessarily orthogonal, and  $q_0 + q_1 = 1$ . We show that circuits (i)–(iv) of Fig. 6(b) all lead to the same probability for the outcome  $z$ .

The controlled- $U$  in circuit (i) transforms the input state to

$$\sqrt{q_0}|\psi_0\rangle \otimes |0\rangle + \sqrt{q_1}U|\psi_1\rangle \otimes |1\rangle, \quad (2.12)$$

and the subsequent Hadamard gate,  $H$ , leaves the state

$$\frac{1}{\sqrt{2}}\left(\sqrt{q_0}|\psi_0\rangle + \sqrt{q_1}U|\psi_1\rangle\right) \otimes |0\rangle + \frac{1}{\sqrt{2}}\left(\sqrt{q_0}|\psi_0\rangle - \sqrt{q_1}U|\psi_1\rangle\right) \otimes |1\rangle, \quad (2.13)$$



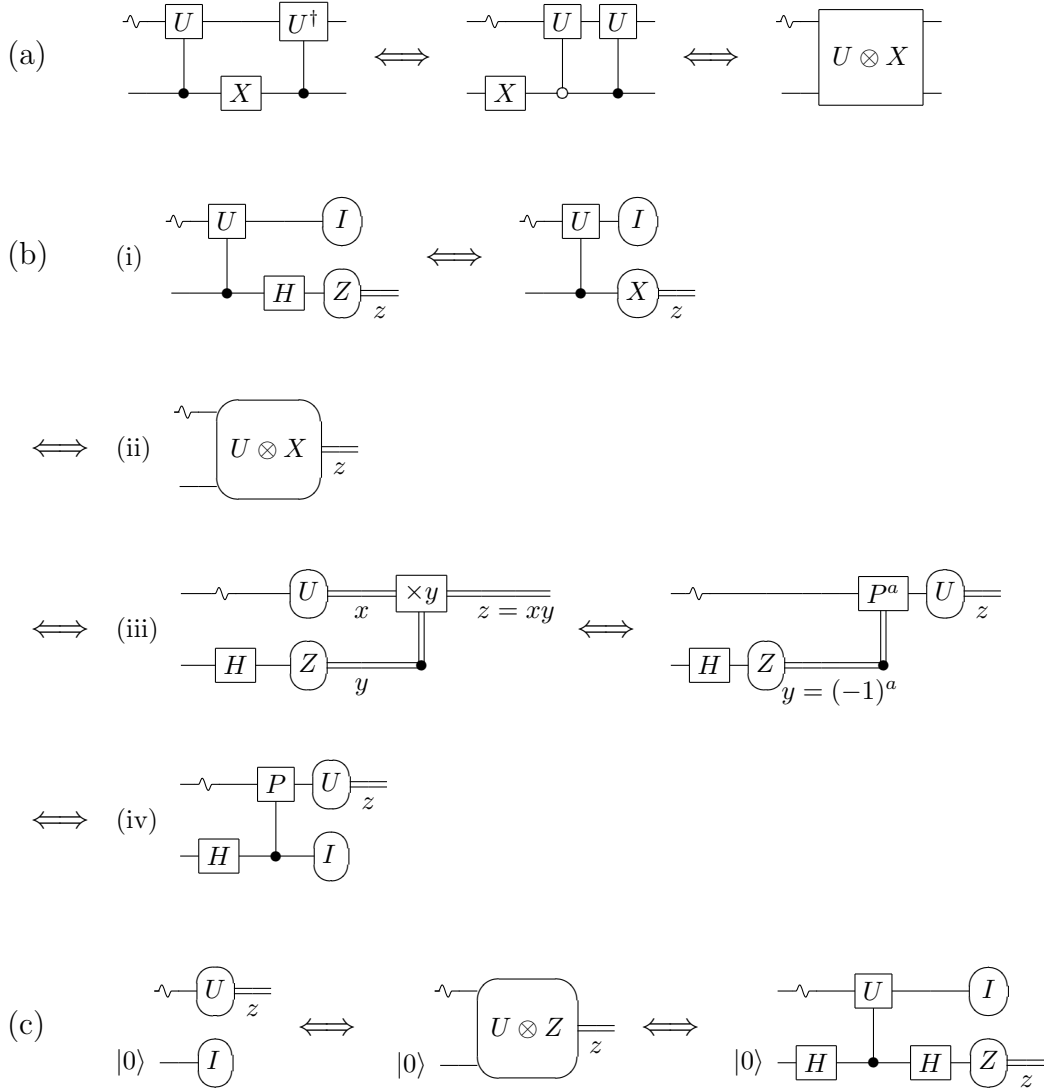


FIG. 6: The unitary operator  $U$  is also Hermitian, i.e.,  $U = U^\dagger$ , implying that all its eigenvalues are equal to  $\pm 1$ . (a) Conjugation of  $I \otimes X$  by a controlled- $U$  gives  $U \otimes X$ . In the middle circuit,  $X$  has been pushed through the initial controlled- $U$ , turning the control on  $|1\rangle$  to control on  $|0\rangle$ . (b) Circuit equivalences for disentangling circuits. The first two steps unitarily transform the measurement of  $I \otimes Z$  to  $U \otimes X$ . The next step reverts to a  $Z$  measurement preceded by a Hadamard and includes explicit classical control circuitry for multiplying the outcomes of the  $U$  and  $Z$  measurements. The fourth step uses the bottom equivalence in Fig. 5(b) to replace the post-measurement classical multiplication, which swaps  $\pm 1$  outcomes, with a pre-measurement unitary  $P$  that swaps the  $\pm 1$  eigenspaces of  $U$ , i.e.,  $PUP^\dagger = -U$ . This step thus requires that the  $\pm 1$  eigenspaces have the same dimensions. The final step uses the principle of deferred measurement of Fig. 5(c) to move the controlled operation through the  $Z$  measurement. The labels (i)–(iv) are introduced for later reference. That (i)–(iv) all lead to the same probability for the ultimate outcome  $z$  is worked out in detail in the text. (c) Measurement of  $U$ , achieved with the use of an ancillary qubit. The first equivalence is true because the qubit’s input state is  $|0\rangle$ . The second equivalence follows from using  $Z = HXH$  twice, surrounding an application of the equivalence in (a). The result is a standard method for measuring parity  $\Pi$ . Notice that this part does not require that  $U$  have  $\pm 1$  eigenspaces of the same dimension.

from which it follows that the probability to obtain outcome  $z$  in the  $Z$  measurement on the qubit is

$$p_z = \left\| \sqrt{q_0}|\psi_0\rangle + z\sqrt{q_1}U|\psi_1\rangle \right\|^2 = \frac{1}{2} \left( 1 + 2z\sqrt{q_0q_1} \operatorname{Re}(\langle\psi_0|U|\psi_1\rangle) \right). \quad (2.14)$$

For circuit (ii), the probability for outcome  $z$  follows from the expectation value of  $U \otimes X$  in the input state (2.11), i.e.,

$$p_z = \frac{1}{2} (1 + z\langle\psi|U \otimes X|\psi\rangle) = \frac{1}{2} \left( 1 + z\sqrt{q_0q_1} (\langle\psi_0|U|\psi_1\rangle + \langle\psi_1|U|\psi_0\rangle) \right), \quad (2.15)$$

which is the same as Eq. (2.14) because  $U = U^\dagger$ .

In circuit (iii), the state after the initial Hadamard takes the form

$$\sqrt{r_{+1}} \frac{1}{\sqrt{2r_{+1}}} \left( \sqrt{q_0}|\psi_0\rangle + \sqrt{q_1}|\psi_1\rangle \right) \otimes |0\rangle + \sqrt{r_{-1}} \frac{1}{\sqrt{2r_{-1}}} \left( \sqrt{q_0}|\psi_0\rangle - \sqrt{q_1}|\psi_1\rangle \right) \otimes |1\rangle, \quad (2.16)$$

where

$$r_y = \left\| \sqrt{q_0}|\psi_0\rangle + y\sqrt{q_1}|\psi_1\rangle \right\|^2 = \frac{1}{2} \left( 1 + 2y\sqrt{q_0q_1} \operatorname{Re}(\langle\psi_0|\psi_1\rangle) \right) \quad (2.17)$$

is the probability for the  $Z$  measurement to yield outcome  $y$ . The state of the mode after the  $Z$  measurement yields outcome  $y$  is

$$\frac{1}{\sqrt{2r_y}} \left( \sqrt{q_0}|\psi_0\rangle + y\sqrt{q_1}|\psi_1\rangle \right). \quad (2.18)$$

Hence, the conditional probability for the measurement of  $U$  to have outcome  $x$ , given outcome  $y$  for the  $Z$  measurement, is

$$\begin{aligned} p_{x|y} &= \frac{1}{2} \left( 1 + x \left( \begin{array}{c} \text{expectation value} \\ \text{of } U, \text{ given } y \end{array} \right) \right) \\ &= \frac{1}{2} \left( 1 + x \frac{1}{2r_y} \left( \sqrt{q_0}\langle\psi_0| + y\sqrt{q_1}\langle\psi_1| \right) U \left( \sqrt{q_0}|\psi_0\rangle + y\sqrt{q_1}|\psi_1\rangle \right) \right) \\ &= \frac{1}{2} \left( 1 + \frac{x}{2r_y} \left( q_0\langle\psi_0|U|\psi_0\rangle + q_1\langle\psi_1|U|\psi_1\rangle \right) + \frac{xy\sqrt{q_0q_1}}{r_y} \operatorname{Re}(\langle\psi_0|U|\psi_1\rangle) \right). \end{aligned} \quad (2.19)$$

The unconditioned probability for the outcome of the  $U$  measurement is

$$p_x = \sum_y p_{x|y} r_y = \frac{1}{2} \left( 1 + x \left( q_0\langle\psi_0|U|\psi_0\rangle + q_1\langle\psi_1|U|\psi_1\rangle \right) \right). \quad (2.20)$$

In contrast, the conditional probability for the product of the two outcomes,  $z = xy$ , is  $p_{z|y} = p_{x=zy|y}$ , which gives an unconditioned probability

$$p_z = \sum_y p_{x=zy|y} r_y = \frac{1}{2} \left( 1 + 2z\sqrt{q_0q_1} \operatorname{Re}(\langle\psi_0|U|\psi_1\rangle) \right), \quad (2.21)$$

the same as that in Eq. (2.14).

In circuit (iv), after the initial Hadamard and the controlled- $P$ , the state becomes

$$\frac{1}{\sqrt{2}} \left( \sqrt{q_0}|\psi_0\rangle + \sqrt{q_1}|\psi_1\rangle \right) \otimes |0\rangle + \frac{1}{\sqrt{2}} P \left( \sqrt{q_0}|\psi_0\rangle - \sqrt{q_1}|\psi_1\rangle \right) \otimes |1\rangle. \quad (2.22)$$

Hence, the probability of outcome  $z$  in the measurement of  $U$  is

$$\begin{aligned}
p_z &= \frac{1}{2} \left( 1 + z \frac{1}{2} \left( \sqrt{q_0} \langle \psi_0 | + \sqrt{q_1} \langle \psi_1 | \right) U \left( \sqrt{q_0} | \psi_0 \rangle + \sqrt{q_1} | \psi_1 \rangle \right) \right. \\
&\quad \left. + z \frac{1}{2} \left( \sqrt{q_0} \langle \psi_0 | - \sqrt{q_1} \langle \psi_1 | \right) P U P^\dagger \left( \sqrt{q_0} | \psi_0 \rangle - \sqrt{q_1} | \psi_1 \rangle \right) \right) \\
&= \frac{1}{2} \left( 1 + 2z \sqrt{q_0 q_1} \operatorname{Re}(\langle \psi_0 | U | \psi_1 \rangle) \right), \tag{2.23}
\end{aligned}$$

where the final step uses that  $P$  conjugates  $U$  to its opposite, i.e.,  $P U P^\dagger = -U$ . The final probability is again the same as that in Eq. (2.14).

There is an important special case of these four demonstrations, typical of interferometric settings and instructive in figuring out how these circuits work. Suppose that all inputs to the circuit have the form (2.11), with  $|\psi_0\rangle$  and  $|\psi_1\rangle$  being orthogonal, but with a relative phase  $\phi$  between  $|\psi_0\rangle$  and  $|\psi_1\rangle$ . Thus the inputs take the form

$$\sqrt{q_0} |\psi_0\rangle \otimes |0\rangle + \sqrt{q_1} e^{-i\phi} |\psi_1\rangle \otimes |1\rangle. \tag{2.24}$$

We can apply all our results for the three circuits simply by making the replacement  $|\psi_1\rangle \rightarrow e^{-i\phi} |\psi_1\rangle$ . The phase  $\phi$ , which can be thought of as the phase to be estimated in an interferometer, is encoded in the entanglement of the upper wire of the circuit with the qubit on the lower wire. Furthermore, suppose that  $U$  swaps  $|\psi_0\rangle$  and  $|\psi_1\rangle$ , i.e.,  $U|\psi_0\rangle = |\psi_1\rangle$  and  $U|\psi_1\rangle = |\psi_0\rangle$ . If we think of  $|\psi_0\rangle$  and  $|\psi_1\rangle$  as the standard states in a two-dimensional Hilbert space, then  $U$  is the Pauli  $X$  operator in this space, and  $P$  can be chosen to be the Pauli  $Z$  operator.

In this situation it is clear that circuit (ii) employs a joint measurement to read out the phase information directly. In circuit (i), the role of the controlled- $U$  is to disentangle the upper and lower wires, leaving the product state  $|\psi_0\rangle \otimes (\sqrt{q_0}|0\rangle + \sqrt{q_1}e^{-i\phi}|1\rangle)$ , in which the phase information is written on the qubit. The subsequent Hadamard transfers the phase information to amplitude information, which determines the outcome probabilities for the measurement of  $Z$ . Likewise, in circuit (iv), the state after the Hadamard and controlled- $P$  is a product state,  $(\sqrt{q_0}|\psi_0\rangle + \sqrt{q_1}e^{-i\phi}|\psi_1\rangle) \otimes (|0\rangle + |1\rangle)/\sqrt{2}$ , but in this case, the phase information is written onto the top line of the circuit. Circuits (i) and (iv) are thus both disentangling circuits, which write the phase information onto one of the quantum wires, where it can be read out by a measurement on that wire alone. For both circuits, the probability of outcome  $z$  is  $p_z = \frac{1}{2}(1 + 2z\sqrt{q_0 q_1} \cos \phi)$ .

Circuit (iii) is also disentangling, but works in a different way. With the current assumptions, the two outcomes of the measurement of  $Z$  are equally likely, i.e.,  $r_y = 1/2$ , and the state of the upper wire after the measurement of  $Z$  yields outcome  $y$  is  $\sqrt{q_0}|\psi_0\rangle + y\sqrt{q_1}e^{-i\phi}|\psi_1\rangle$ . The upper wire now carries the phase information, but one needs the outcome  $y$  to know how to extract phase information from the subsequent measurement of  $U$ . The conditional probability for the outcome  $x$  of the  $U$  measurement, given  $y$ , is  $p_{x|y} = \frac{1}{2}(1 + 2xy\sqrt{q_0 q_1} \cos \phi)$ . If one does not use the outcome  $y$ , then the phase produces no interference, the unconditioned probability for  $x$  being  $p_x = 1/2$ , but if one does use the phase information, as in the classical control of circuit (iii), the phase does produce interference, the unconditioned probability for the product,  $z = xy$ , being the same as for circuits (i), (ii), and (iv).

In circuits (i) and (iv), disentanglement occurs as a consequence of coherent operations, but in circuit (iii), disentanglement is a consequence of the measurement of  $Z$ . This measurement-induced (or post-selected) disentanglement was originally called a *quantum eraser* [41, 42, 43]; the modern understanding is that what is “erased” is the entanglement that destroys interference when one measures only the top wire or the bottom wire. A nice feature of the circuit (iii) is that one can regard the Hadamard and measurement of  $Z$  as occurring either before or after the

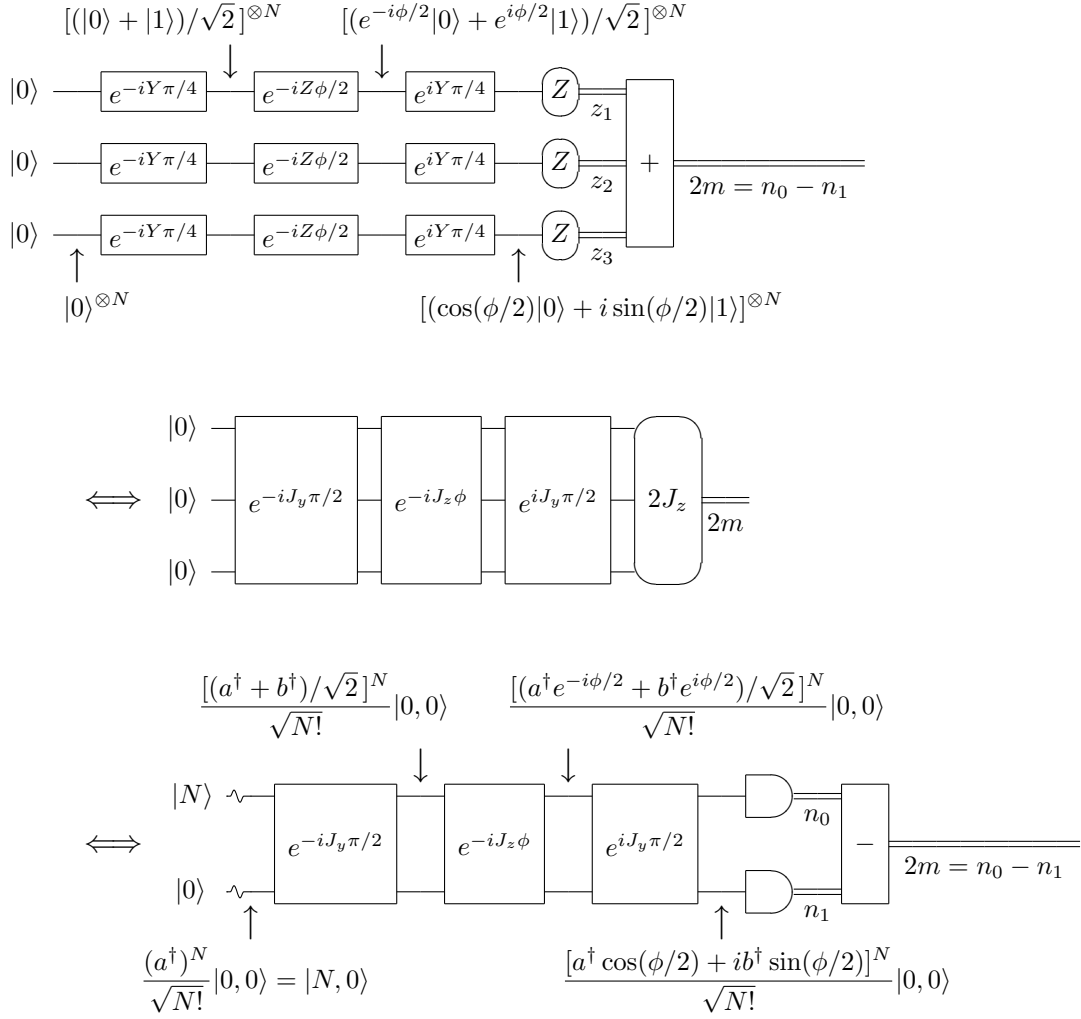


FIG. 7: Conventional qubit and equivalent modal interferometers, which use independent particles. The top circuit, a qubit interferometer, clearly acts independently on the input qubits, subjecting each to a  $\pi/2$  pulse, a rotation that imposes the phase  $\phi$ , and a second  $\pi/2$  pulse. The state of the  $N$  qubits after each gate is given. Each qubit is measured in the standard basis; the probabilities to be found in states  $|0\rangle$  and  $|1\rangle$  are  $\cos^2(\phi/2)$  and  $\sin^2(\phi/2)$ . The  $N$  outputs are processed to extract the difference  $2m = n_0 - n_1$ . The middle circuit writes the same interferometer in terms of Schwinger operators, and the bottom circuit completes the translation to a modal description. The  $N$  photons, initially all in mode 0, are subjected to a 50/50 beamsplitter, a phase shifter, and a second 50/50 beamsplitter, after which the number of photons in each mode is counted, with the outputs differenced to produce  $2m = n_0 - n_1$ . Quantum states are again tracked after each gate. The output  $2m$  is binomially distributed; the mean and variance of  $m$  are  $\langle m \rangle = \frac{1}{2}N \cos \phi$  and  $\Delta^2 m = \frac{1}{4}N \sin^2 \phi$ . The resulting phase sensitivity,  $\delta\phi = \Delta m / |d\langle m \rangle / d\phi| = 1/\sqrt{N}$ , is the quantum noise limit. The overall interferometric transformation is a rotation by  $-\phi$  about the  $x$  axis, i.e.,  $e^{iJ_y\pi/2}e^{-iJ_z\phi}e^{-iJ_y\pi/2} = e^{iJ_x\phi}$ .

measurement of  $U$ . In the former case, they seem to prepare a state on the top wire that carries the phase information and in the latter case, they seem to “erase” the entanglement that destroyed the interference on the top wire, but there is no difference between these two cases, only a difference in perspective.

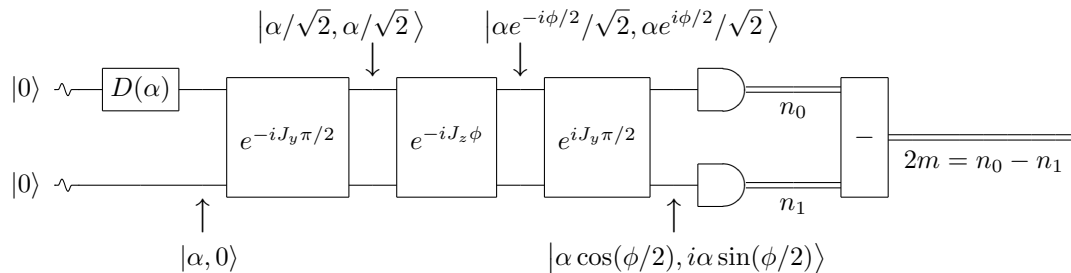


FIG. 8: Coherent-state version of a conventional modal interferometer. The input coherent state  $|\alpha, 0\rangle = D(\alpha) \otimes I|0, 0\rangle = e^{-|\alpha|^2/2} \sum_{N=0}^{\infty} (\alpha^N / \sqrt{N!}) |N, 0\rangle$  is the result of applying the displacement operator  $D(\alpha)$  to the vacuum state of mode 0. The displacement operator is the mathematical description of the action of a classical driving field on the mode; the action of an ideal laser operating far above threshold is well approximated by a displacement operator, apart from a slow drift in phase. Since the interferometer itself is number-preserving, the different  $N$ -photon sectors of the coherent state are processed independently, implying that the output probabilities are obtained by averaging the binomial distribution of Fig. 7 over the coherent state's Poisson distribution for total photon number. The resulting mean and variance of  $m$  are  $\langle m \rangle = \frac{1}{2}|\alpha|^2 \cos \phi$  and  $\Delta^2 m = \frac{1}{4}|\alpha|^2 \sin^2 \phi$ , which gives phase sensitivity  $\delta\phi = 1/|\alpha|$ . We can think of the coherent-state interferometer as a classical interferometer contaminated by the shot noise of the coherent state's Poisson distribution. The classicality of the coherent states appears in the state description, tracked through the gates, as the fact that the phase  $\phi$  appears not as a relative phase between states in superposition, but as a phase change of coherent-state (classical) complex amplitudes.

### III. QUANTUM-NOISE-LIMITED INTERFEROMETERS

The chief purpose of this paper is to examine and relate different methods for achieving Heisenberg-limited sensitivity, i.e., phase sensitivity that scales as  $1/N$  with the number  $N$  of atoms or photons. Before taking up that task in Sec. IV, however, we first look, in Fig. 7, at conventional qubit and modal interferometers, which use independent particles. Qubit interferometers are typically atomic (Ramsey) interferometers, and modal interferometers employ two modes of the electromagnetic field. The sensitivity of a conventional interferometer scales as  $1/\sqrt{N}$ , the so-called *quantum noise limit* (or shot-noise limit) [1].

A couple of aspects of the interferometers in Fig. 7 deserve attention. In the modal version, the input Fock state  $|N\rangle$  for mode 0 can be replaced by a coherent state  $|\alpha\rangle = D(\alpha)|0\rangle$ , where  $D(\alpha) = e^{\alpha a^\dagger - \alpha^* a}$  is the modal displacement operator. It is worth recording that  $e^{-i\mathbf{J}\cdot\hat{\mathbf{n}}\theta} D(\alpha) \otimes D(\beta) e^{i\mathbf{J}\cdot\hat{\mathbf{n}}\theta} = D(\alpha') \otimes D(\beta')$ , where

$$\begin{pmatrix} \alpha' \\ \beta' \end{pmatrix} = M \begin{pmatrix} \alpha \\ \beta \end{pmatrix}, \quad (3.1)$$

with  $M$  given by Eq. (2.6). This implies that

$$e^{-i\mathbf{J}\cdot\hat{\mathbf{n}}\theta} |\alpha, \beta\rangle = |\alpha', \beta'\rangle. \quad (3.2)$$

A coherent-state interferometer is depicted and described in Fig. 8. It is a semi-realistic rendition of what is done in optical interferometry, since an ideal laser produces a very good approximation to a coherent state.

It is clear from both the qubit and modal versions of a conventional interferometer that the output is insensitive to common-mode phase shifts. This is the primary advantage of measuring phase shifts in an interferometric setting. It is also clear, however, that the equatorial axes of

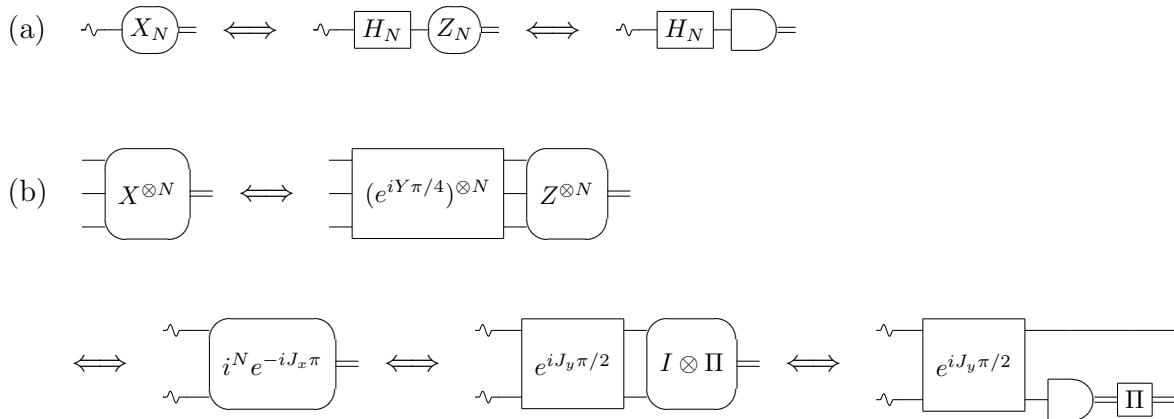


FIG. 9: (a) A measurement of  $X_N = |0\rangle\langle N| + |N\rangle\langle 0|$  is equivalent to an effective Hadamard gate  $H_N = (X_N + Z_N)/\sqrt{2}$  followed by a measurement of  $Z_N = |0\rangle\langle 0| - |N\rangle\langle N|$ . A subscript  $N$  on a two-dimensional unitary operator signifies that operator acting in the “qubit” modal subspace spanned by standard states  $|0\rangle$  and  $|N\rangle$ . The final form, which replaces the measurement of  $Z_N$  by photocounting, is valid if the input state lies in the “qubit” subspace spanned by  $|0\rangle$  and  $|N\rangle$ ; it is an example of extending a measurement outside a subspace of interest. (b) A measurement of  $X^{\otimes N}$  on  $N$  qubits is equivalent to measuring  $i^N e^{-iJ_x\pi}$  on modes, and this in turn is equivalent to a 50/50 beamsplitter followed by a measurement of the parity of mode 1. Notice that  $X^{\otimes N} = i^N e^{-iJ_x\pi}$  is the qubit FLIP and modal SWAP operator:  $i^N e^{-iJ_x\pi}|n_0, n_1\rangle = |n_1, n_0\rangle$ . We use this measurement in our discussion of N00N-state interferometers, where all that is really needed is a measurement of the observable  $|N, 0\rangle\langle 0, N| + |0, N\rangle\langle N, 0|$  in the two-dimensional subspace spanned by  $|N, 0\rangle$  and  $|0, N\rangle$ ;  $i^N e^{-iJ_x\pi}$  is a natural extension of this observable into the entire Hilbert space. Throughout this paper, we symbolize a parity measurement as in the last circuit—photocounting followed by classical extraction of parity—but the reader should remember that Fig. 6(c), with  $U = \Pi$ , provides another, standard circuit for measuring parity, by mapping the parity to an ancillary qubit.

the two 50/50 beamsplitters (or  $\pi/2$  transitions) must be well defined relative to one another. A change in the equatorial axis of the second beamsplitter introduces a relative phase shift across the beamsplitter that is indistinguishable from the phase  $\phi$ . In most applications, where one is only interested in changes in  $\phi$ , the actual requirement is that the relative phase shifts across the two beamsplitters be stable relative to one another over times somewhat longer than the time scale of changes in  $\phi$ .

In different implementations, the stability requirements between the two beamsplitters assume different forms. In optical-frequency interferometers, where the modes typically correspond to different spatial paths or different polarizations, the phase shifts across the beamsplitters are determined by coatings on the beamsplitters and by placement or orientation of the beamsplitters; it is relatively easy to keep these stable. In atomic interferometers, the relative phase shifts across the  $\pi/2$  pulses are chiefly determined by the times at which the pulses are applied; it is not difficult to keep the time separating the two pulses stable at microwave frequencies.

#### IV. FOCK-STATE-SUPERPOSITION INTERFEROMETERS

Entanglement among particles allows one to improve the sensitivity scaling for estimating a phase beyond that offered by the quantum noise limit. The optimal sensitivity scaling, known as the *Heisenberg limit*, is given by  $1/N$  [13, 14, 15]. There are many different methods for achieving this limit, most of which involve using superpositions of two Fock states of one or two modes. In

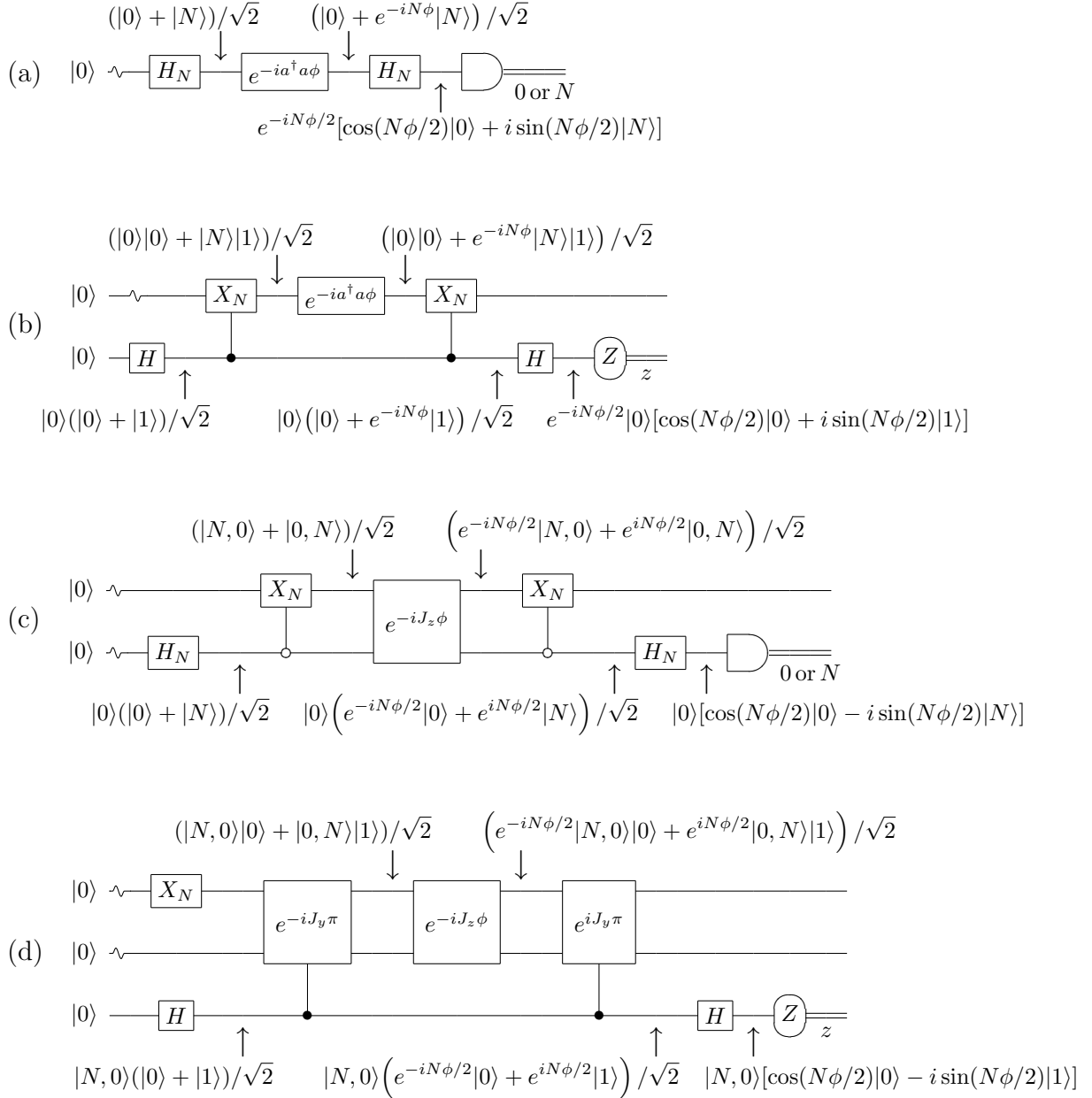


FIG. 10: Four Heisenberg-limited phase-estimation protocols that use Fock-state superpositions: (a) single-mode phase estimation; (b) single-mode, qubit-assisted phase estimation, (c) two-mode interferometer, called a N00N interferometer after the state before the phase shifter; (d) two-mode, qubit-assisted interferometer. In the qubit-assisted protocols, the qubit can be thought of as a second or third arm of an interferometer. Quantum states are tracked through each protocol. In protocols (b) and (d), inserting a gate  $e^{i\theta/2}e^{-iZ\theta/2}$  between the two controls on the qubit wire shifts the fringe pattern by angle  $\theta$ ; in particular, an  $S$  gate shifts the fringes by  $\pi/2$ . In protocols (a) and (c), the output is either 0 photons or  $N$  photons; mapping 0 to  $+1$  and  $N$  to  $-1$ , the outcome becomes  $z = \pm 1$ , as in protocols (b) and (d). In all cases, the probabilities of the two outcomes are  $p_z = \frac{1}{2}(1 + z \cos N\phi)$ . The mean and variance of  $z$ ,  $\langle z \rangle = \cos N\phi$  and  $\Delta^2 z = \sin^2 N\phi$ , give Heisenberg-limited phase sensitivity  $\delta\phi = \Delta z / |d\langle z \rangle / d\phi| = 1/N$ . The photocounting in the N00N interferometer (c) can be replaced by a measurement of  $Z_N$ . Then the operations after the phase shifter are equivalent to a measurement of  $X_N \otimes X_N$ , which for the N00N-state input, is the same as a measurement of  $|N, 0\rangle\langle 0, N| + |0, N\rangle\langle N, 0|$ ; this, in turn, as pointed out in Fig. 9(b), is equivalent on N00N-state inputs to a measurement of the modal SWAP operator  $i^N e^{-iJ_x \pi}$ .

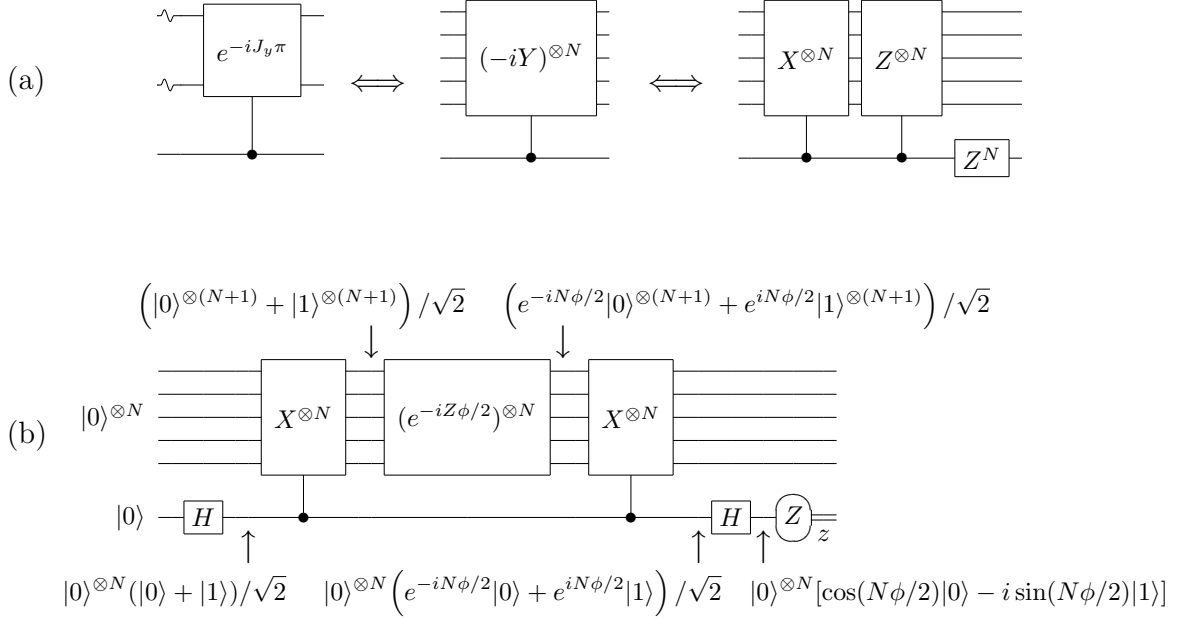


FIG. 11: (a) Circuit equivalences that equate a controlled-SWAP between two modes to controlled-NOTs and controlled-SIGNs on  $N = 5$  qubits, plus a  $Z^N$  on the control qubit. (b)  $N$ -qubit cat-state interferometer, obtained by applying (a) to the two-mode, qubit-assisted interferometer in Fig. 10(d). The interferometer is named after the cat state  $(|0\rangle^{\otimes(N+1)} + |1\rangle^{\otimes(N+1)})/\sqrt{2}$  at the input to the phase shifters; it has the same outcome probabilities and phase sensitivity as Fig. 10(d). Proposals for cat-state interferometers often also apply the phase shift to the control qubit; that does not happen here because of the special role of the control qubit, which is inherited from the two-mode, qubit-assisted circuit in Fig. 10(d).

this section we consider four such methods and use circuit equivalences to show they are equivalent. In Sec. V, we turn to corresponding methods that use superpositions of coherent states and find that they, too, saturate the Heisenberg limit, but with considerably better prospects for realization in the laboratory.

Before getting started on Fock-state-superposition interferometers, we introduce two measurement rules in Fig. 9. The first, in Fig. 9(a), is useful in our discussion of phase estimation using a single mode, and the second, in Fig. 9(b), comes into play when we discuss genuine interferometers, which use two modes, such as N00N-state interferometers. In the first rule, we introduce the notation that a subscript  $N$  on a two-dimensional unitary operator denotes that operator acting in the “qubit” modal subspace spanned by standard states  $|0\rangle$  and  $|N\rangle$ . The second rule is important for interferometers because it converts a measurement of the modal SWAP operator into a measurement that might be doable, i.e., a measurement of the parity of one mode behind a 50/50 beamsplitter.

The ability to convert to a parity measurement—and its importance—has been appreciated in many papers [5, 7, 9, 10, 11, 17, 44, 45]. Parity can be measured by photocounting followed by classical extraction of the parity—this is how we represent a parity measurement throughout this paper—but it can also be measured using the protocol of Fig. 6(c) with  $U = \Pi$ , which maps the parity to an ancillary qubit, and by other methods that rely on the interference of two modes [46, 47, 48]. Indeed, these methods can be applied more generally to measuring the displaced parity operator, a measurement that comes up naturally in our discussion in Sec. V, and that is the basis for direct measurements of the Wigner function of a mode [21, 22, 39, 40, 46, 47, 48, 49].



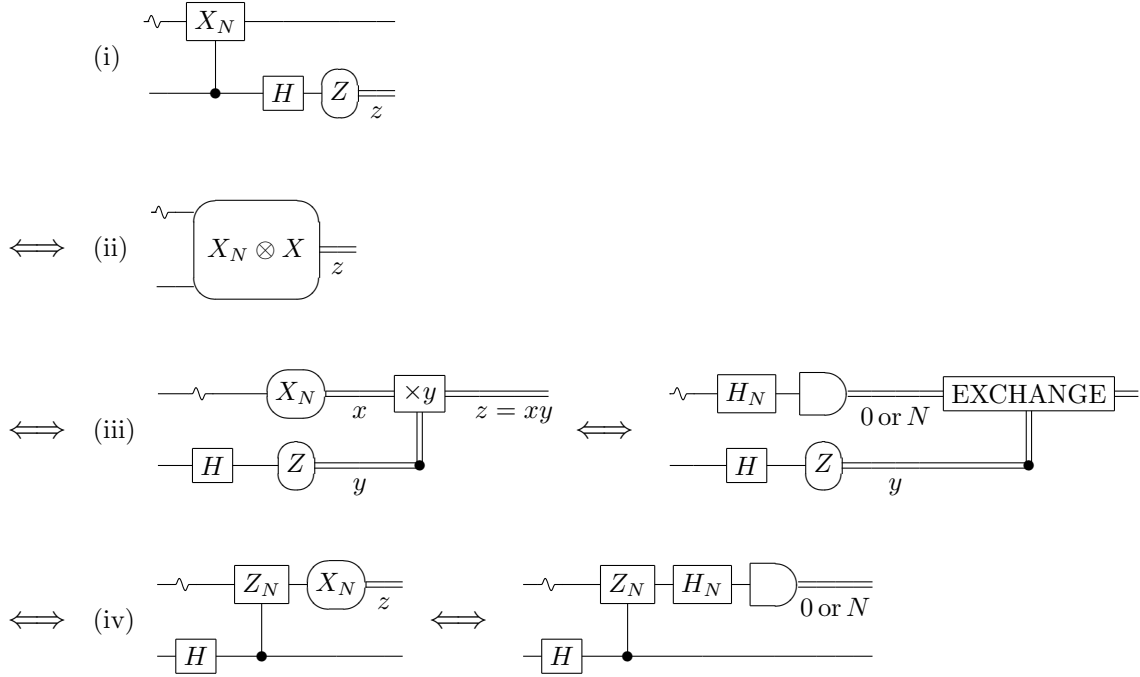


FIG. 12: Circuit equivalences for disentangling circuits when the unitary  $U$  of Fig. 6(b) is  $X_N$ . Circuits are numbered as in Fig. 6(b). Circuits (iii) and (iv) are converted to more useful forms by replacing the measurement of  $X_N$  by an effective Hadamard followed by photocounting, as in Fig. 9(a). In (iii), the classical controlled-EXCHANGE swaps the outcomes 0 and  $N$  when the outcome of the  $Z$  measurement is  $y = +1$ . In (iv),  $Z_N$  is the operator that conjugates  $X_N$  to its opposite.

Figure 10 depicts circuit diagrams, labeled (a)–(d), for four phase-estimation protocols that employ superpositions of two Fock states. It is clear from the tracking of quantum states through these protocols that they are closely related and that all achieve Heisenberg-limited sensitivity by having a fringe pattern that oscillates  $N$  times as fast as the independent-particle fringe pattern of a conventional interferometer. We emphasize that these methods differ from conventional interferometry in that they are not committed to placing beamsplitters immediately before and after the phase shifter, as in a conventional interferometer, but rather allow any procedure for preparing the input state to the phase shifter and any measurement procedure after the beamsplitter.

Of the four protocols in Fig. 10, the best known is interferometer (c), which inputs N00N states,  $(|N, 0\rangle + |0, N\rangle)/\sqrt{2}$ , to the differential phase shifter  $e^{-iJ_z\phi}$  and thus can be called a N00N interferometer [5, 6, 7, 8, 9, 10, 11, 12]. We remind the reader that the two-mode, qubit-assisted interferometer (d) is equivalent to an  $N$ -qubit cat-state interferometer [2, 3, 4], as is shown in Fig. 11.

The easiest equivalence to show is that of circuits (b) and (c). Insert a  $Z$  at the beginning of the qubit wire in (b). Push it to the end of the circuit through the measurement, thereby converting the controlled operations to control on  $|0\rangle$ . Replace the qubit with the two-dimensional modal subspace spanned by standard states  $|0\rangle$  and  $|N\rangle$ . Insert an irrelevant global phase  $e^{iN\phi/2}$ ; this changes the phase shift  $e^{-ia^\dagger a\phi}$  on mode 0 to a differential phase shift  $e^{-iJ_z\phi}$  and completes the conversion of (b) to (c).

The other equivalences, (b) to (a) and (d) to (c), are more interesting. It is easy to see that circuit (b) is a version of (a) with the phase information carried by an entangled state of the

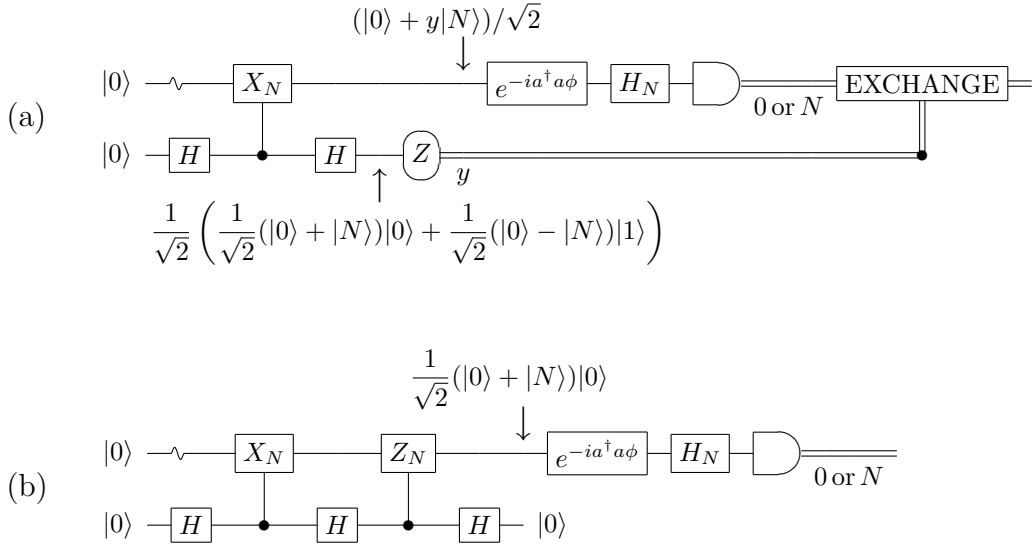


FIG. 13: (a) Version of the circuit of Fig. 10(a) obtained by applying the second form of circuit (iii) in Fig. 12 to the circuit of Fig. 10(b). In this version, the superposition state input to the phase shifter is prepared by post-selection based on the outcome of the  $Z$  measurement on the qubit. The two possible outcomes occur with equal probability; the two input states,  $(|0\rangle \pm |N\rangle)/\sqrt{2}$ , produce fringe patterns that are  $\pi$  out of phase. Averaging over outcomes destroys the fringe pattern, but the classical control circuitry restores a single fringe pattern. The initial circuitry and qubit measurement entangle and then disentangle the mode and the qubit; if the qubit measurement is regarded as occurring after the photocounting, this is the action of a quantum eraser. (b) Version of the circuit of Fig. 10(a) obtained by applying the second form of circuit (iv) in Fig. 12 to the circuit of Fig. 10(b). Since  $Z_N$  commutes with  $a^\dagger a$ , the controlled- $Z_N$  passes unscathed through the phase shifter, becoming part of a coherent procedure for the superposition state input to the phase shifter. A final Hadamard gate is added to the qubit wire to return the qubit to its initial state  $|0\rangle$ .

mode and the qubit; likewise, circuit (d) is a version of (c) with the phase information carried by entanglement of the two modes with the qubit. In the qubit-assisted protocols, (b) and (d), the post-phase-shift operations write all the phase information onto the qubit by disentangling it from the mode(s), whereas in (a) and (c), the phase information is on the mode(s). The key to showing the equivalences is thus to use the disentangling equivalences of Fig. 6(b) to move the phase information in (b) and (d) onto the mode(s) instead of onto the qubit.

Figures 12–15 demonstrate the two equivalences; the demonstration that (d) is equivalent to (c) is very closely analogous to the demonstration that (b) is equivalent to (a). Figures 12 and 14 specialize the disentangling circuits of Fig. 6(b) to the situations in circuits (b) and (d), and Figs. 13 and 15 apply these to circuits (b) and (d) to convert them to versions of (a) and (c). The converted circuits have particular procedures, assisted by the qubit, for preparing an appropriate input state to the phase shifter. These preparation procedures are either post-selected, i.e., based on the outcome of a measurement on the qubit, or completely coherent. They require the ability to make  $N$ -photon states and to control two-dimensional Fock-state subspaces, both of which are very hard to do experimentally. Attempts to make N00N states beyond  $N = 2$  up till now have had to be nondeterministic [12].

On the other hand, the superposition state that powers (a),  $(|0\rangle + |N\rangle)/\sqrt{2}$ , has been made deterministically for  $N = 1$  to 5 in a qubit/cavity setting, where the qubit is a superconducting cir-

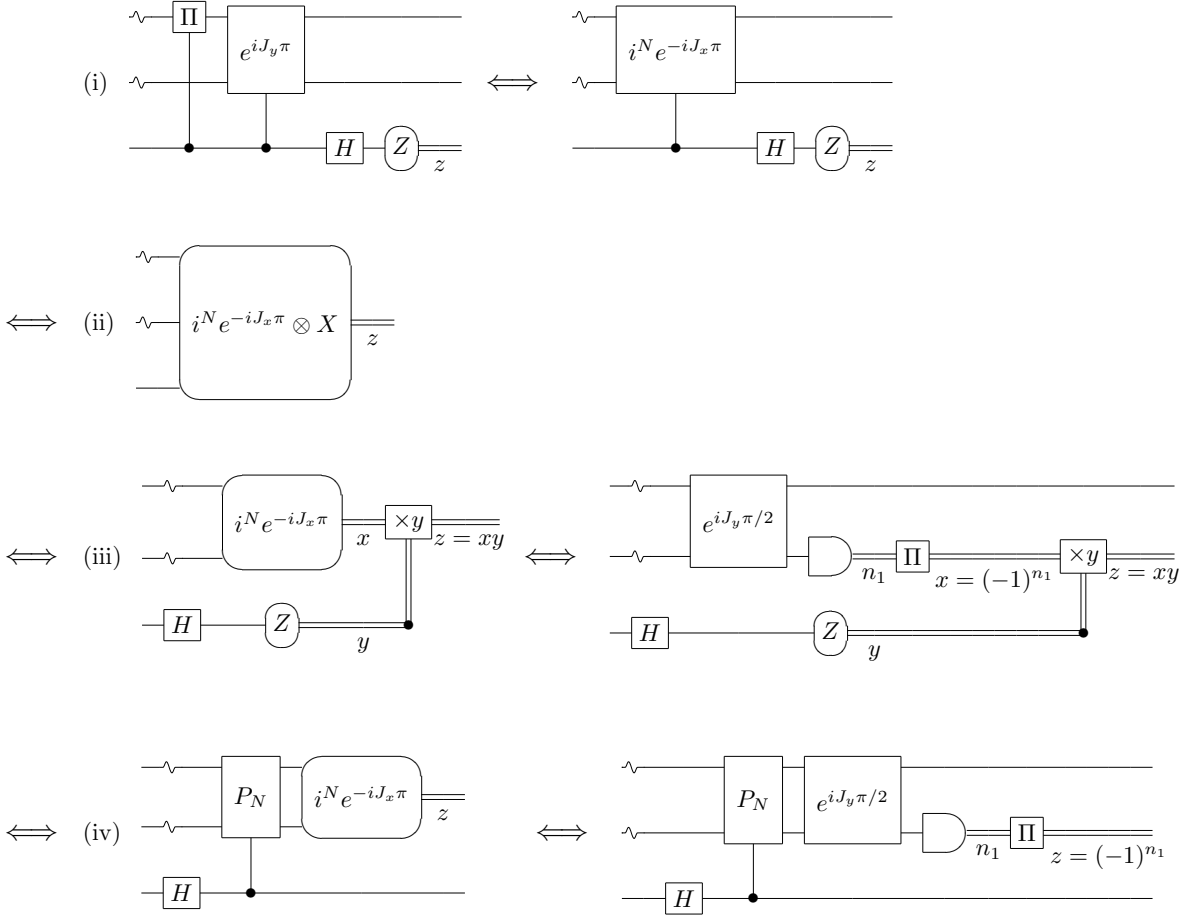


FIG. 14: Circuit equivalences for disentangling circuits when the unitary  $U$  of Fig. 6(b) is  $e^{iJ_y\pi}\Pi \otimes I = i^N Y^{\otimes N} (-Z)^{\otimes N} = X^{\otimes N} = i^N e^{-iJ_x\pi} = e^{-iJ_y\pi/2} I \otimes \Pi e^{iJ_y\pi/2}$ . The controlled- $(\Pi \otimes I)$  is included to make  $U$  Hermitian as well as unitary. Circuits are numbered as in Fig. 6(b). Circuits (iii) and (iv) are converted to more useful forms by replacing the measurement of  $i^N e^{-iJ_x\pi}$  by a 50/50 beamsplitter followed by photocounting on mode 1 and classical extraction of parity, as in Fig. 9(b). The step to circuit (iv) is not generally valid, since it requires that the  $\pm 1$  eigenspaces of  $i^N e^{-iJ_x\pi}$  have the same dimension, which is only true when  $N$  is odd. We use circuit (iv), however, only when the modal inputs are confined to the subspace spanned by  $|N, 0\rangle$  and  $|0, N\rangle$ ; in this case we can define  $P_N$  by  $P_N|N, 0\rangle = |N, 0\rangle$  and  $P_N|0, N\rangle = -|0, N\rangle$ . When  $N$  is odd, we can choose  $P_N = I \otimes \Pi$ .

circuit and the mode belongs to a microwave-frequency resonator [49]. The state-preparation protocol used in that experiment, due to Law and Eberly [50], can be used in principle to create arbitrary superpositions of resonator Fock states. It alternates rotations of the qubit with carefully timed Rabi couplings of the qubit to the resonator to deposit successive photons in the resonator mode. This protocol does not lend itself readily to the circuit notation of this paper, nor in its reliance on a ladder of two-level transitions, is it an efficient method for making large- $N$  superpositions  $(|0\rangle + |N\rangle)/\sqrt{2}$ .

Gerry and Campos [7] have proposed a realization of the post-selected preparation procedure of Fig. 15(a). The role of the qubit is taken over by two field modes that carry a single photon, and the controlled- $e^{-iJ_y\pi}$  is achieved by a cross-Kerr coupling, which does a controlled swap of the coupled modes.

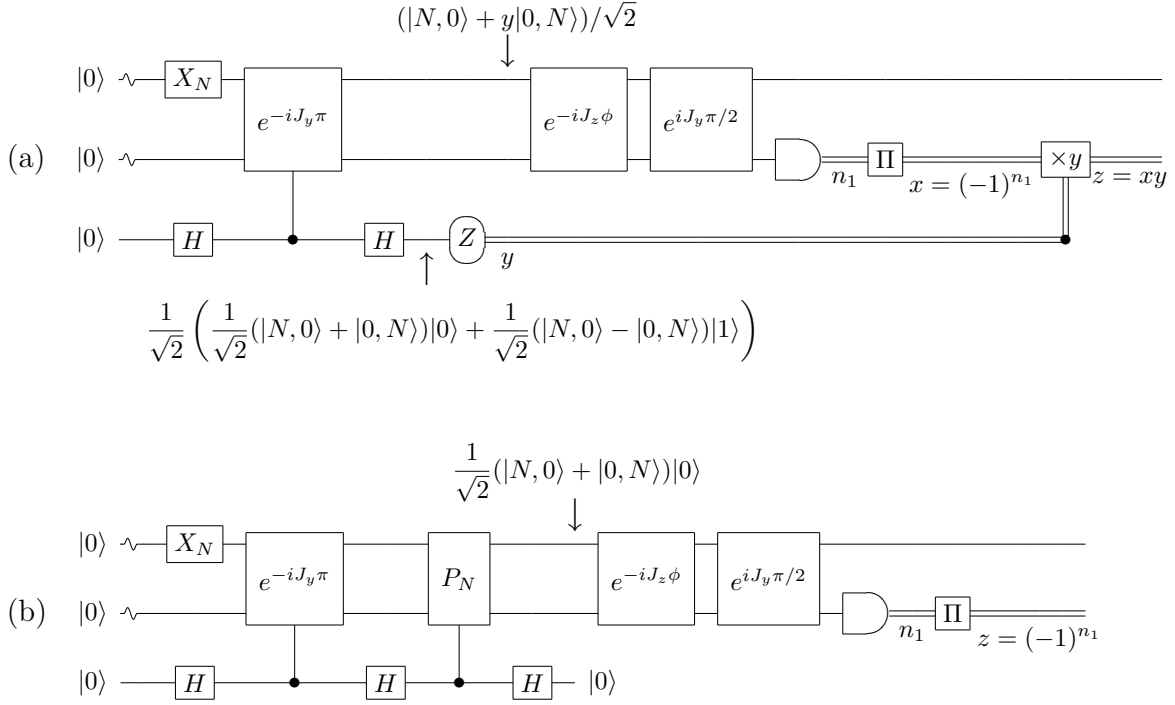


FIG. 15: (a) Version of the N00N circuit of Fig. 10(c) obtained by applying the second form of circuit (iii) in Fig. 14 to the circuit of Fig. 10(d). The controlled- $(I \otimes \Pi)$  at the beginning of Fig. 14(i) is moved to the beginning of Fig. 14(iii); it is pushed through the phase shifter and then through the controlled- $e^{-iJ_y\pi}$ , becoming a controlled- $(I \otimes \Pi)$  [because  $\Pi \otimes I e^{-iJ_y\pi} = (-Z)^{\otimes N} (-iY)^{\otimes N} = (-iY)^{\otimes N} Z^{\otimes N} = e^{-iJ_y\pi} I \otimes \Pi$ ], which can be omitted on mode 1's vacuum input. In this version, the superposition state input to the phase shifter is prepared by post-selection based on the outcome of the  $Z$  measurement on the qubit. The two possible outcomes occur with equal probability; the two N00N inputs,  $(|N, 0\rangle \pm |0, N\rangle)/\sqrt{2}$ , produce fringe patterns that are  $\pi$  out of phase. Averaging over outcomes destroys the fringe pattern, but the classical control circuitry restores a single fringe pattern. The initial circuitry and qubit measurement entangle and then disentangle the modes and the qubit; if the qubit measurement is regarded as occurring after the photocounting, this is the action of a quantum eraser. (b) Version of the N00N circuit of Fig. 10(c) obtained by applying the second form of circuit (iv) in Fig. 14 to the circuit of Fig. 10(d). The controlled- $(\Pi \otimes I)$  is handled as in (a). Since  $P_N$  commutes with  $J_z$ , the controlled- $P_N$  passes through the phase shifter, becoming part of a coherent procedure for the superposition state input to the phase shifter. A final Hadamard gate is added to the qubit wire to return the qubit to its initial state  $|0\rangle$ . The measurement procedure in (a) and (b)—50/50 beamsplitter followed by photocounting and classical extraction of parity—doesn't look like the measurement procedure in Fig. 10(c), but both procedures are equivalent to measuring the modal SWAP operator,  $i^N e^{-iJ_x\pi}$ , as noted in Figs. 9 and 10.

## V. COHERENT-STATE-SUPERPOSITION INTERFEROMETERS

Just as for conventional interferometers, we can turn a Heisenberg-limited interferometer from one that uses superpositions of Fock states to a corresponding one that uses superpositions of coherent states. In this section, we take the single-mode and two-mode, qubit-assisted protocols of Fig. 10(b) and (d) and convert them to run on coherent states. We then apply disentangling measurement equivalences to convert to protocols that prepare input states to the phase shifter that are superpositions of two coherent states. For a single mode, a superposition of two coherent states is often called a cat state, but we refer to it as a *modal cat state* to distinguish it from the

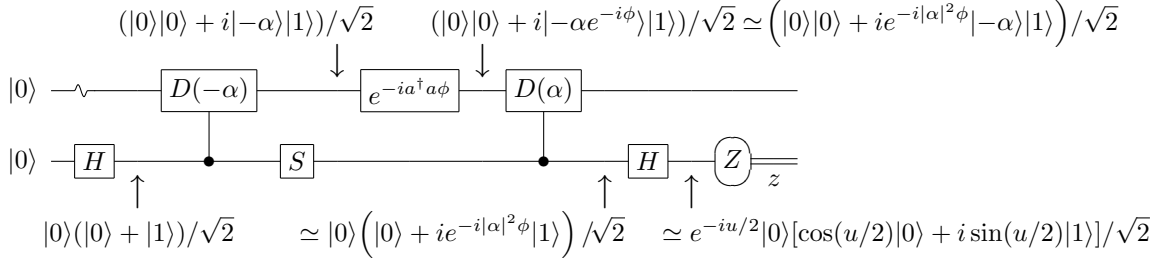


FIG. 16: Coherent-state analogue of the single-mode, qubit-assisted phase-estimation protocol in Fig. 10(b). In constructing the analogue, one replaces the two controlled- $X_N$ s with controlled displacements that are inverses of one another. Here we make the first a controlled- $D(-\alpha)$  and the second a controlled- $D(\alpha)$ . We also introduce an  $S$  gate on the qubit to shift the fringe pattern by  $\pi/2$  so that optimal sensitivity occurs at  $\phi = 0$ ; this fringe shift turns out to fit naturally into further manipulations of the circuit. Quantum states are tracked through the circuit. An approximately equal sign ( $\simeq$ ), here and henceforth, indicates an expression that assumes small phase shifts,  $|\alpha|^2\phi^2 \ll |\alpha|^2\phi \ll 1$ . The approximate expressions emphasize the similarity to Fig. 10(b); exact expressions are given in the text. In the final state, we use the variable  $u = |\alpha|^2\phi - \pi/2$  for brevity; it expresses the  $\pi/2$  phase shift produced by the  $S$  gate. For small phase shifts, the probability of outcome  $z$  is  $p_z \simeq \frac{1}{2}[1 + z \sin(|\alpha|^2\phi)]$ , which gives Heisenberg-limited sensitivity  $\delta\phi = 1/|\alpha|$ .

cat state of  $N$  qubits.

Versions of our preparation procedures for superpositions of coherent states turn out to be practical, at least at microwave frequencies. Ultimately, there are two features that make coherent superpositions more practical than Fock-state superpositions. First, coherent states have their own phase, which we can play with in addition to the relative phase in superpositions; second, coherent states can be created and manipulated by coherent driving fields, represented by the displacement operator, thus providing an additional, crucial transformation that is not useful when dealing with Fock states.

### A. Single-mode coherent-state-superposition phase estimation

Figure 16 gives the coherent-state analogue of the single-mode, qubit-assisted protocol of Fig. 10(b). The state after the controlled- $D(\alpha)$  is

$$\frac{1}{\sqrt{2}} \left( |0\rangle|0\rangle + iD(\alpha)|-\alpha e^{-i\phi}\rangle|1\rangle \right). \quad (5.1)$$

It is easy to work out that

$$D(\alpha)|-\alpha e^{-i\phi}\rangle = D(\alpha)e^{-ia^\dagger a \phi}D(-\alpha)|0\rangle = e^{-i|\alpha|^2 \sin \phi} |\alpha(1 - e^{-i\phi})\rangle, \quad (5.2)$$

from which one finds that

$$\langle 0|D(\alpha)|-\alpha e^{-i\phi}\rangle = \langle \alpha|e^{-ia^\dagger a \phi}|\alpha\rangle = e^{-|\alpha|^2(1-e^{-i\phi})} = e^{-i|\alpha|^2 \sin \phi} e^{-2|\alpha|^2 \sin^2(\phi/2)}. \quad (5.3)$$

In the small-angle approximation,  $|\alpha|^2\phi^2 \ll |\alpha|^2\phi \ll 1$ , the state (5.2) has negligible overlap with any Fock state other than the vacuum state and thus is given approximately by  $D(\alpha)|-\alpha e^{-i\phi}\rangle \simeq e^{-i|\alpha|^2\phi}|0\rangle$ . Written in a slightly different way, this becomes

$$|\alpha e^{-i\phi}\rangle = e^{-ia^\dagger a \phi}|\alpha\rangle \simeq e^{-i|\alpha|^2\phi}|\alpha\rangle. \quad (5.4)$$

This is the approximation used in the state tracking of Fig. 16. It says that a small phase shift of a coherent state simply places an appropriate phase in front of the coherent state; it expresses the fact that for the Fock states with appreciable amplitude in a coherent state, the phase shifts differ by roughly  $|\alpha|\phi = |\alpha|^2\phi/|\alpha|$ , which for small phase shifts is negligible compared to the average phase shift  $|\alpha|^2\phi$ .

The probability for the  $Z$  measurement on the qubit to yield outcome  $z$  is  $p_z = \frac{1}{2}(1 + \langle Z \rangle)$ . The expectation value of  $Z$  in the final state is the same as that for  $X$  in the state (5.1) before the final Hadamard. Thus this probability is given by

$$\begin{aligned} p_z &= \frac{1}{2} \left[ 1 - z \operatorname{Im} \left( \langle 0 | D(\alpha) | -\alpha e^{-i\phi} \rangle \right) \right] \\ &= \frac{1}{2} \left( 1 + z \sin(|\alpha|^2 \sin \phi) e^{-2|\alpha|^2 \sin^2(\phi/2)} \right) \\ &\simeq \frac{1}{2} \left( 1 + z \sin(|\alpha|^2 \phi) \right) . \end{aligned} \tag{5.5}$$

The final expression holds in the small-angle approximation and leads to Heisenberg-limited sensitivity for small phase shifts.

A controlled displacement, like those in Fig. 16, was introduced as a potential operation by Davidovich and co-workers [19, 20], who called it a *quantum switch*, because a qubit coherently switches a classical driving field on a mode. These papers suggested that a quantum switch might be realized at microwave frequencies in a qubit/cavity set-up like that in Serge Haroche's Paris laboratory [23, 24]: a rubidium atom occupying one of two Rydberg levels, which constitute the qubit, passes through a superconducting microwave cavity; one level does not interact with the microwave field, but the other dispersively switches a cavity mode into resonance with a classical driving field, which excites the mode into a coherent state.

Although a quantum switch has not been implemented in the laboratory, the same effect can be achieved by using a closely related procedure, depicted in Fig. 17, which employs a sequence of displacements and controlled parities. A controlled-II is a particular case of a controlled phase shift, with the phase shift set to  $\pi$ . Such controlled phase shifts have been implemented in the atom/cavity setting, with the dispersive coupling of one Rydberg level simply phase shifting the cavity mode. Such controlled phase shifts were proposed and analyzed in the atom/cavity setting in Ref. [18]. Initial experiments [23, 51] had small phase shifts, but recent experimental work in Haroche's group takes advantage of large controlled phase shifts,  $\pi/4$  [52, 53] and  $\pi$  [54, 55], produced in times much shorter than the cavity's damping time. The phase-estimation procedure of Fig. 16, with the quantum switch replaced by the equivalent procedure of Fig. 17, has been proposed and analyzed for implementation in the atom/cavity setting by Toscano and co-authors [56].

Our next task is to convert the qubit-assisted protocol of Fig. 16 to forms that have procedures for making modal cat states as input to the phase shifter. In this endeavor, Fig. 18 specializes the first three disentangling equivalences of Fig. 6(b) to the protocol of Fig. 16, and Fig. 19 gives protocols in which the input state to the phase shifter is a modal cat state.

The circuit in Fig. 19(a) uses post-selection: it prepares one of two modal cat states,  $|\psi_y\rangle = (|0\rangle + iy|\alpha\rangle)/\sqrt{2}$ , depending on which of the two equally likely outcomes  $y$  eventuates from the  $Z$  measurement on the qubit. The cat states are the relative states,  $|\psi_0\rangle$  and  $|\psi_1\rangle$ , of the extended discussion in Sec. IIB; they are normalized, but not orthogonal, having a purely imaginary inner product  $\langle \psi_- | \psi_+ \rangle = i\langle 0 | \alpha \rangle = ie^{-|\alpha|^2/2}$ .

The protocol of Fig. 19(a) is precisely equivalent to that of Fig. 16, since it is derived by using the disentangling equivalences of Fig. 18 to disentangle the qubit from the mode in Fig. 16. The state just before the photocounter,

$$|\psi'_y\rangle = \frac{1}{\sqrt{2}} D(-\alpha/2) \left( |0\rangle + iy|\alpha e^{-i\phi}\rangle \right) , \tag{5.6}$$

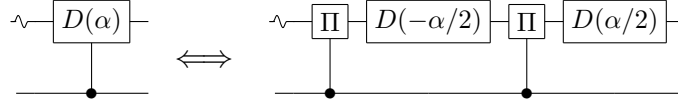


FIG. 17: A quantum switch, in which a qubit coherently switches a classical driving field, is equivalent to a sequence of displacements and controlled parities, as one easily verifies using  $D(\alpha/2)\Pi D(-\alpha/2) = D(\alpha)\Pi$ . A controlled- $\Pi$  is a particular case of controlled phase shift, with the phase shift set to  $\pi$ . The first controlled- $\Pi$  can be omitted if the input state of the mode has even parity (e.g., the vacuum state). In our circuit diagrams, we often use the quantum switch because it is more compact, but the equivalent procedure is more realistic, at least at microwave frequencies, where the necessary controlled operations have been implemented in the laboratory.

can be used to calculate the probability for outcome  $x$  of the parity measurement,  $p_{x|y} = \frac{1}{2}(1 + x\langle\psi'_y|\Pi|\psi'_y\rangle)$ . The expectation value of parity is

$$\langle\psi'_y|\Pi|\psi'_y\rangle = \frac{1}{2}\left(\langle 0|\alpha\rangle + \langle\alpha e^{-i\phi}|D(\alpha)|-\alpha e^{-i\phi}\rangle\right) - y\text{Im}\left(\langle 0|D(\alpha)|-\alpha e^{-i\phi}\rangle\right). \quad (5.7)$$

We need

$$\langle\alpha e^{-i\phi}|D(\alpha)|-\alpha e^{-i\phi}\rangle = e^{-i|\alpha|^2 \sin\phi} \langle\alpha e^{-i\phi}|\alpha(1 - e^{-i\phi})\rangle = e^{-|\alpha|^2/2} e^{-4|\alpha|^2 \sin^2(\phi/2)}. \quad (5.8)$$

Putting all this together, we get a conditional probability

$$\begin{aligned} p_{x|y} &= \frac{1}{2}\left(1 + \frac{1}{2}xe^{-|\alpha|^2/2}(1 + e^{-4|\alpha|^2 \sin^2(\phi/2)}) + xy \sin(|\alpha|^2 \sin\phi) e^{-2|\alpha|^2 \sin^2(\phi/2)}\right) \\ &\simeq \frac{1}{2}\left(1 + xe^{-|\alpha|^2/2} + xy \sin(|\alpha|^2 \phi)\right), \end{aligned} \quad (5.9)$$

where the second expression assumes small phase shifts. As in the general discussion in Sec. II B, averaging over  $y$  yields an unconditioned probability for  $x$  that has no  $\phi$ -dependence, but the product variable,  $z = xy$ , reveals a fringe pattern, with the unconditioned probability  $p_z$  given by Eq. (5.5).

The protocol of Fig. 19(b) uses a coherent procedure to prepare the cat state  $|\psi_+\rangle$ . It is easy to see that the probability for outcome  $z$  is given by Eq. (5.9) with  $y = +1$  and  $x = z$ . This probability is not the same as Eq. (5.5), signaling that the circuit of Fig. 19(b) is not quite equivalent to Fig. 16, though it becomes effectively so when  $|\alpha|$  is large, so that  $|0\rangle$  and  $|\alpha\rangle$  are nearly orthogonal.

Both circuits in Fig. 19 prepare modal cat states for input to the phase shifter, (a) by post-selection and (b) coherently. There is an independent coherent method for preparing a modal cat state, which does not require assistance from a qubit, relying instead on a self-Kerr coupling. This method, which goes back to the pioneering work of Yurke and Stoler [57], follows mathematically from the simple identity  $e^{-in^2\pi/2} = e^{-i\pi/4}e^{i(-1)^n\pi/4} = e^{-i\pi/4}[1 + i(-1)^n]\sqrt{2}$ , which implies that a self-Kerr coupling, with a  $\pi/2$  phase shift, makes a modal cat state:

$$e^{-i(a^\dagger a)^2\pi/2}|\alpha\rangle = e^{-|\alpha|^2} \sum_{n=0}^{\infty} \frac{\alpha^n e^{-in^2\pi/2}}{\sqrt{n!}}|n\rangle = \frac{e^{-i\pi/4}}{\sqrt{2}}(|\alpha\rangle + i|-\alpha\rangle). \quad (5.10)$$

The use of Kerr and higher-order nonlinearities to make cat states and more complicated superpositions of coherent states has been elaborated extensively [58, 59].

Methods for preparing modal cat states by post-selection have been proposed using quantum switches [19, 20] and using controlled phase shifts and controlled nonlinear interactions [5, 60,

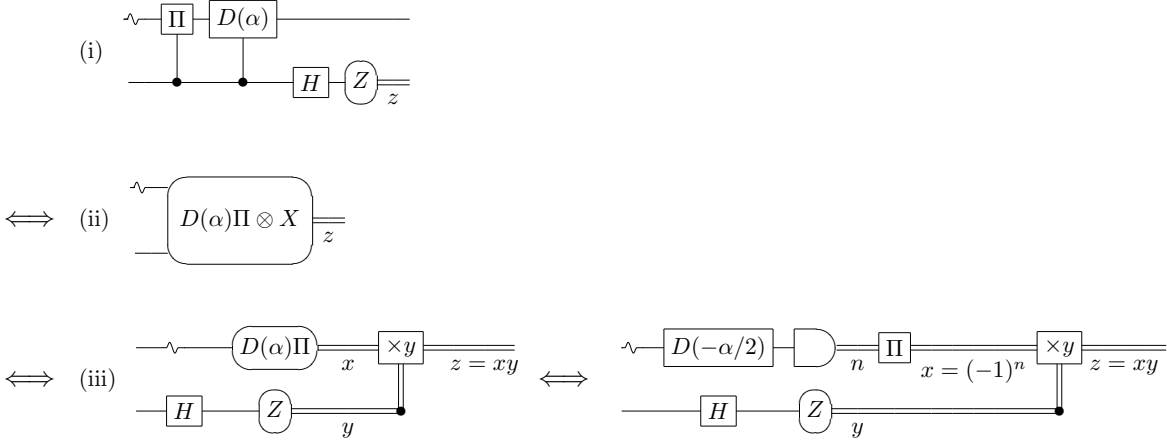


FIG. 18: Circuit equivalences for disentangling circuits when the unitary  $U$  of Fig. 6(b) is  $D(\alpha)\Pi = D(\alpha/2)\Pi D(-\alpha/2)$ . The controlled- $\Pi$  is included to make  $U$  Hermitian as well as unitary. Circuits are numbered as in Fig. 6(b), but circuit (iv) is omitted because it is more productive to guess a coherent preparation procedure to go with Fig. 16 than to determine an operator  $P$  that conjugates  $D(\alpha)\Pi$  to its opposite. Circuit (iii) is converted to a more useful form by replacing the measurement of  $D(\alpha)\Pi$  by a displacement followed by photocounting and classical extraction of parity.

61], and these have been applied to the cat-state interferometer [5] of Fig. 19(a). Dalvit and co-workers [62] have investigated post-selected preparation of more elaborate superpositions of coherent states, such as superpositions of four coherent states, called compass states [63], for use in interferometers of this sort. The superpositions are created using quantum switches and Kerr interactions; the emphasis is on preparation procedures that might be implemented in an ion trap, where the qubit is two internal levels of an ion and the mode is a vibrational mode. In earlier work, Schneider and co-workers [64] reported methods for making such superpositions of coherent states in an ion trap.

## B. Two-mode coherent-state-superposition interferometers

Having dealt with single-mode phase estimation, we turn now to the two-mode, qubit-assisted protocol of Fig. 10(d). Figure 20 translates that Fock-state-superposition protocol into a corresponding coherent-state-superposition protocol. The translation replaces the preparation procedure of Fig. 10(d) with a procedure that uses two quantum switches to make the appropriate mode-qubit entangled state, as proposed in Refs. [19, 20]. The rest of the circuit remains the same, except for the addition of an  $S$  gate on the qubit wire, which shifts the fringe pattern by  $\pi/2$  so that  $\phi = 0$  is an optimal operating point. This turns out to be a natural addition, just as in Sec. V A. The final state provides the probability for outcome  $z$ ,

$$\begin{aligned}
 p_z &= \frac{1}{4} \left| \left| |\alpha e^{-i\phi/2}\rangle + iz|\alpha e^{i\phi/2}\rangle \right| \right|^2 \\
 &= \frac{1}{2} \left[ 1 + z \text{Im} \left( \langle \alpha | e^{-ia^\dagger a \phi} | \alpha \rangle \right) \right] \\
 &= \frac{1}{2} \left( 1 - z \sin(|\alpha|^2 \sin \phi) e^{-2|\alpha|^2 \sin^2(\phi/2)} \right), \tag{5.11}
 \end{aligned}$$

which gives Heisenberg-limited sensitivity for small phase shifts.



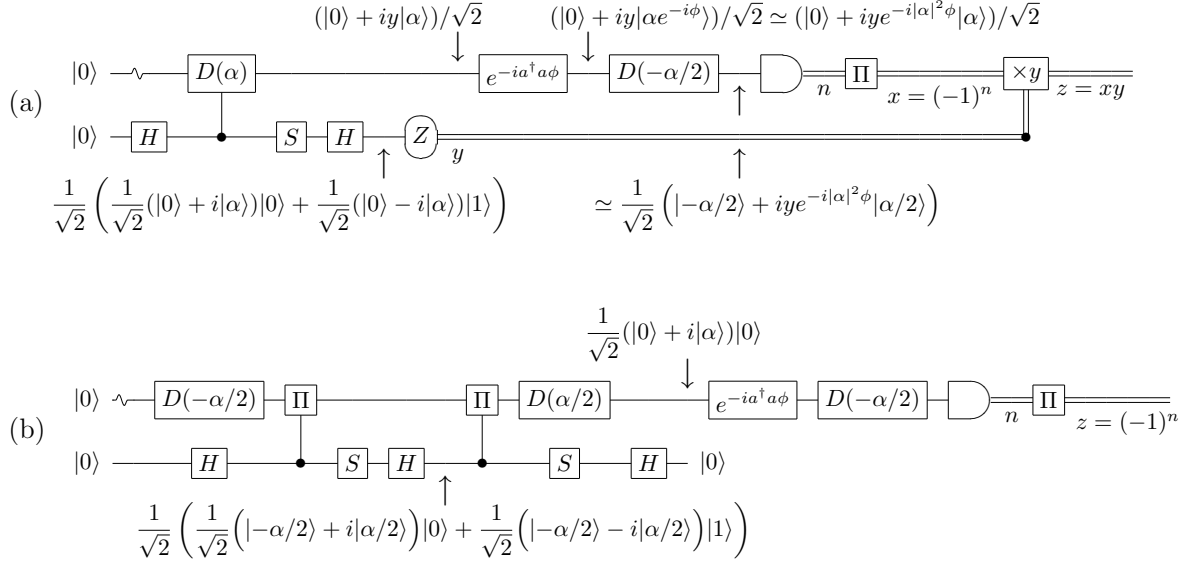


FIG. 19: (a) Circuit obtained by applying the second form of circuit (iii) in Fig. 18 to the circuit of Fig. 16. The controlled- $\Pi$  at the beginning of Fig. 18(i) is moved to the beginning of Fig. 18(iii). It is pushed through the phase shifter,  $S$  gate, and controlled- $D(-\alpha)$ , converting the last to a controlled- $D(\alpha)$ ; it then can be omitted on the mode’s vacuum input. The superposition state input to the phase shifter is prepared by post-selection based on the outcome  $y$  of the  $Z$  measurement on the qubit. The two possible outcomes occur with equal probability; the two input states,  $|\psi_{\pm}\rangle = (|0\rangle \pm i|\alpha\rangle)/\sqrt{2}$ , are normalized, but not orthogonal modal cat states. The final state of the mode before photocounting is given in the small-angle approximation; exact expressions appear in the text. For small phase shifts, the conditional probability for parity outcome  $x$  is  $p_{x|y} = \frac{1}{2}(1 + x\langle\Pi\rangle_y) \simeq \frac{1}{2}[1 + xe^{-|\alpha|^2/2} + xy\sin(|\alpha|^2\phi)]$ . Averaging over  $y$  destroys the fringe pattern, but the classical control circuitry restores a fringe pattern for  $z = xy$ , with probability  $p_z \simeq \frac{1}{2}(1 + z\sin(|\alpha|^2\phi))$ , which gives Heisenberg-limited sensitivity  $\delta\phi = 1/|\alpha|$ . (b) Circuit that coherently prepares modal cat state  $|\psi_+\rangle$  as input to the phase shifter. Since  $D(\alpha/2)\Pi D(-\alpha/2)$  swaps  $|0\rangle$  and  $|\alpha\rangle$ , we have  $D(\alpha/2)\Pi D(-\alpha/2)|\psi_{\pm}\rangle = \pm i|\psi_{\mp}\rangle$ . Thus we can disentangle the mode and qubit and prepare  $|\psi_+\rangle$  by inserting a controlled- $\Pi$ , preceded by  $D(-\alpha/2)$  and succeeded by  $D(\alpha/2)$ , just before the qubit measurement in (a), which can then be omitted. Replacing the quantum switch by its equivalent from Fig. 17 and adding terminal  $S$  and Hadamard gates to the qubit, thereby returning the qubit to its initial state  $|0\rangle$ , yields the circuit shown. We did not use circuit equivalences to obtain this coherent circuit, so it is not precisely equivalent to Fig. 16 and to (a). For small phase shifts, the probability for outcome  $z$  is  $p_z \simeq \frac{1}{2}[1 + ze^{-|\alpha|^2/2} + z\sin(|\alpha|^2\phi)]$ , which reduces to the outcome probability in Fig. 16 and in (a) when  $|\alpha|$  is large.

The next task is to convert the qubit-assisted protocol of Fig. 20 to forms that have procedures for making the appropriate mode-entangled states,  $(|\alpha, 0\rangle \pm i|0, \alpha\rangle)/\sqrt{2}$ , as input to the differential phase shifter. The resulting circuits are given in Fig. 21. In CMC’s research group at the University of New Mexico, we have taken to referring to these states as 0BB0 states (pronounced “oboe”), because we often write them (unnormalized) as  $|0, \beta\rangle + |\beta, 0\rangle$  [65]. We have analyzed the performance of 0BB0 states under losses and considered schemes for implementation, all of which is to be presented elsewhere [66].

The circuit in Fig. 21(a) uses post-selection: it prepares one of the two 0BB0 states,  $|\Psi_y\rangle = (|\alpha, 0\rangle + iy|0, \alpha\rangle)/\sqrt{2}$ , depending on which of the two (equally likely) outcomes  $y$  emerges from the  $Z$  measurement on the qubit. The two 0BB0 states are normalized, but they are not orthogonal, their inner product,  $\langle\Psi_-|\Psi_+\rangle = i|\langle 0|\alpha\rangle|^2 = ie^{-|\alpha|^2}$ , being purely imaginary.

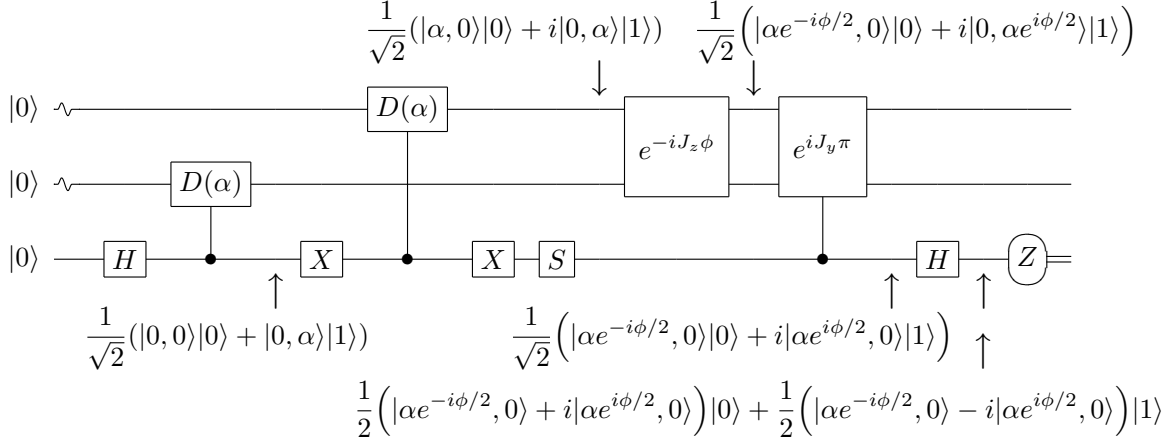


FIG. 20: Coherent-state analogue of two-mode, qubit-assisted interferometer in Fig. 10(d). To create the entangled state input to the differential phase shifter, the circuit uses two quantum switches, the first controlled on  $|1\rangle$  and the second, via the surrounding  $X$  gates, effectively controlled on  $|0\rangle$ . An  $S$  gate on the qubit shifts the fringe pattern by  $\pi/2$  so that optimal sensitivity occurs at  $\phi = 0$ . The entangled state input to the beamsplitter is a superposition of the states at the beamsplitter in Fig. 10(d), with coherent-state amplitudes in the superposition and with the extra  $i$  to shift the fringe pattern. Since the remainder of the circuit preserves photon number, the outcome probability for  $z$  can be obtained by averaging the probability in Fig. 10(d) (with a  $\pi/2$  phase shift),  $\frac{1}{2}(1 - z \sin N\phi)$ , over the coherent-state Poisson distribution for  $N$ ; the result is the distribution (5.11), which gives Heisenberg-limited sensitivity for small phase shifts.

The circuit of Fig. 21(a) is precisely equivalent to that of Fig. 20, since it can be derived from Fig. 20 using the disentangling equivalences of Fig. 14. The state just before the photodetector,

$$|\Psi'_y\rangle = \frac{1}{\sqrt{2}} \left( |\alpha e^{-i\phi/2}/\sqrt{2}, -\alpha e^{-i\phi/2}/\sqrt{2}\rangle + iy |\alpha e^{i\phi/2}/\sqrt{2}, \alpha e^{i\phi/2}/\sqrt{2}\rangle \right), \quad (5.12)$$

provides the probability for outcome  $x$  of the parity measurement,  $p_{x|y} = \frac{1}{2}(1 + x\langle\Psi'_y|I \otimes \Pi|\Psi'_y\rangle)$ , via the expectation value of the parity of mode 1,

$$\begin{aligned} \langle\Psi'_y|I \otimes \Pi|\Psi'_y\rangle &= \langle 0|\sqrt{2}\alpha\rangle + \text{Im}\left(\langle\alpha/\sqrt{2}|e^{-ia^\dagger a\phi}|\alpha/\sqrt{2}\rangle^2\right) \\ &= e^{-|\alpha|^2} - y \sin(|\alpha|^2 \sin \phi) e^{-2|\alpha|^2 \sin^2(\phi/2)}. \end{aligned} \quad (5.13)$$

Thus the conditional probability is

$$p_{x|y} = \frac{1}{2} \left( 1 + x e^{-|\alpha|^2} - xy \sin(|\alpha|^2 \sin \phi) e^{-2|\alpha|^2 \sin^2(\phi/2)} \right) \simeq \frac{1}{2} \left( 1 + x e^{-|\alpha|^2} - xy \sin(|\alpha|^2 \phi) \right), \quad (5.14)$$

where the second expression is valid for small phase shifts. Although the unconditioned probability for  $x$  does not depend on  $\phi$ , a fringe pattern appears in the product variable,  $z = xy$ , whose unconditioned probability is given by Eq. (5.11).

The corresponding protocol that prepares 0BB0 states coherently is depicted in Fig. 21(b). The probability for outcome  $z$  is given by the conditional probability (5.14) with  $y = +1$  and  $x = z$ . This probability is not the same as the final outcome probability in Fig. 20, telling us that this coherent protocol is not precisely equivalent to the circuits of Fig. 20 and Fig. 21(a). It becomes equivalent when  $|\alpha|$  is large, so that  $|\alpha, 0\rangle$  and  $|0, \alpha\rangle$  are essentially orthogonal.

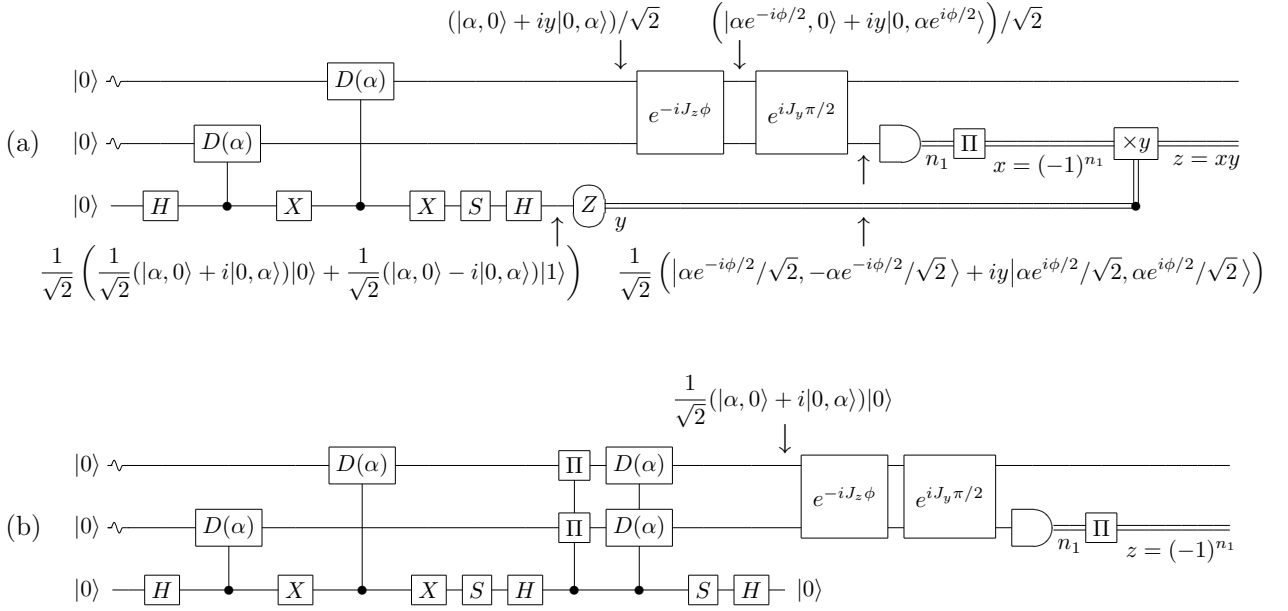


FIG. 21: (a) Circuit obtained by applying the second form of circuit (iii) in Fig. 14 to the circuit of Fig. 20. The controlled- $\Pi$  at the beginning of Fig. 14(i) is shifted to the beginning of Fig. 14(iii). It can be pushed through to just after the initial Hadamard on the qubit wire and can then be omitted on mode 0's vacuum input. The superposition state input to the phase shifter is prepared by post-selection based on the outcome  $y$  of the  $Z$  measurement on the qubit. The two equally likely outcomes produce input OBB0 states,  $|\Psi_{\pm}\rangle = (|\alpha, 0\rangle \pm i|0, \alpha\rangle)/\sqrt{2}$ , which are normalized, but not orthogonal; they are superpositions, with coherent-state amplitudes, of N00N states, but with an additional  $i$  phase shift. Since the remainder of the circuit preserves photon number, we can calculate the probability for outcome  $z$  as a Poisson average of the N00N state probability of Fig. 15(a) (with an additional  $\pi/2$  phase shift),  $p_z = \frac{1}{2}(1 - z \sin N\phi)$ ; the result is the probability  $p_z$  of Eq. (5.11). (b) Circuit that coherently prepares OBB0 state  $|\Psi_{+}\rangle$  as input to the differential phase shifter. Since  $D(\alpha)\Pi$  swaps  $|0\rangle$  and  $|\alpha\rangle$ , we can disentangle the mode and qubit and prepare  $|\Psi_{+}\rangle$  by inserting on both modes a controlled- $\Pi$  followed by a controlled- $D(\alpha)$ . Adding terminal  $S$  and Hadamard gates to the qubit, thereby returning it to its initial state  $|0\rangle$ , gives the circuit shown. Since we did not use circuit equivalences to obtain this coherent circuit, it is not precisely equivalent to Fig. 20 and to (a), though it becomes so when  $|\alpha|$  is large.

The preparation procedure of Fig. 21(b), which employs quantum switches, is converted in Fig. 22(a) to an equivalent protocol that uses controlled parities. This protocol is perhaps a practical way to make an OBB0 state at microwave frequencies because of the ability in an atom/cavity setting to do displacements and controlled phase shifts in times much shorter than the time scale for cavity damping.

Figure 22(b) provides another, entirely independent coherent preparation procedure for OBB0 states, which was proposed by Gerry, Benmoussa, and Campos [9]. This procedure is a nonlinear interferometer, with a self-Kerr coupling in one arm. It generates an OBB0 state by first making a modal cat state with the self-Kerr coupling and using the 50/50 beamsplitters of the interferometer to turn the cat state into an OBB0 state. The nonlinear interferometer preserves photon number and thus can be converted to qubits using the equivalence of Fig. 2(a); the resulting qubit interferometer, which relies on controlled-SIGN gates between all pairs of qubits, is depicted in Fig. 22(c). The equivalent circuits (b) and (c) have been suggested and analyzed by Gerry and Campos [67] as a method for making a N00N-like state in a BEC.

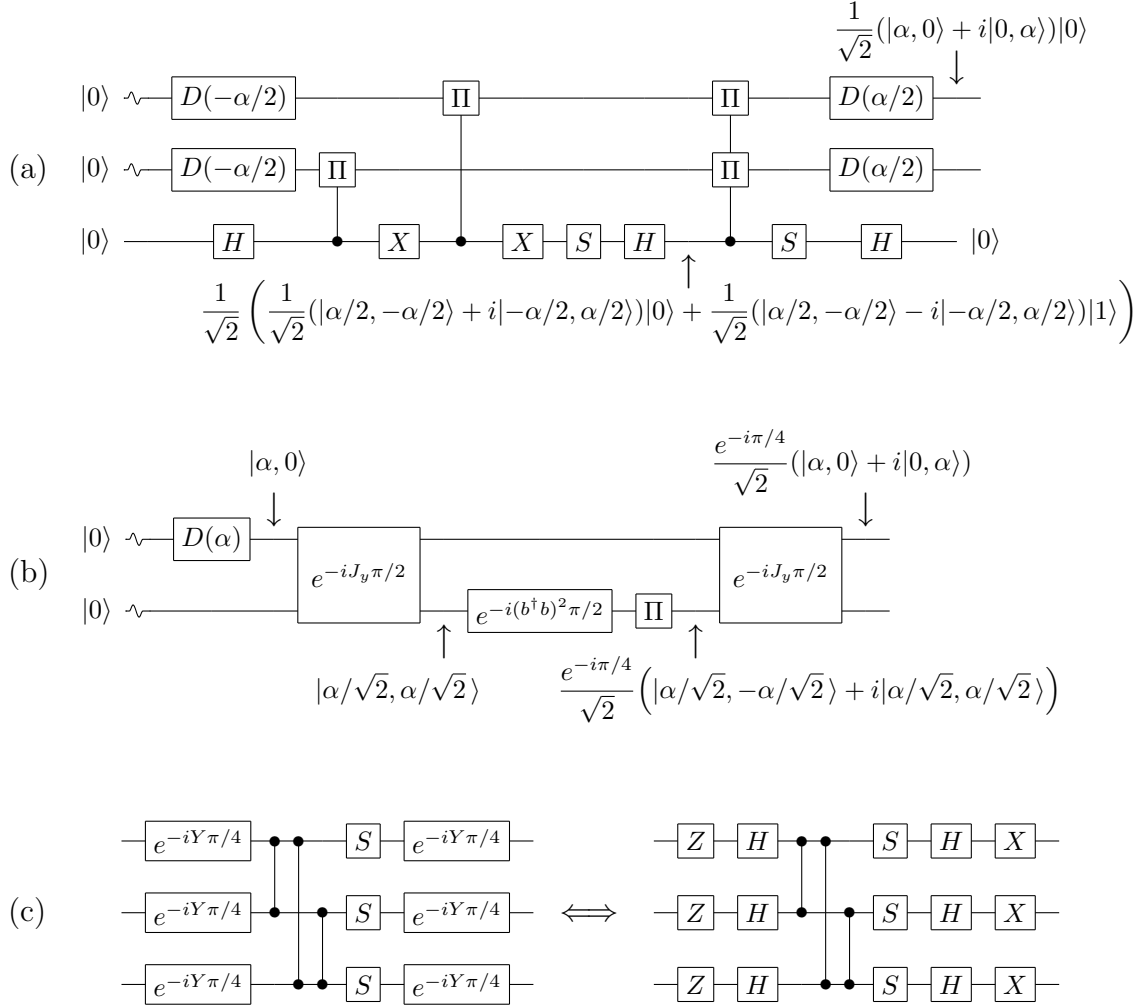


FIG. 22: Coherent preparation procedures for 0BB0 states. (a) The preparation part of the circuit in Fig. 21(b), with quantum switches eliminated in favor of controlled parities by using the equivalence of Fig. 17. (b) Kerr-gate protocol for making 0BB0 states. The circuit is a nonlinear interferometer, with 50/50 beamsplitters before and after a Kerr self-coupling and a  $\pi$  phase shift on mode 1. (c) Translation to  $N = 3$  qubits of the part of circuit (b) after the displacement of mode 0. The translation uses the circuit equivalence of Fig. 2(a); the equivalence uses  $e^{-iY \pi/4} = HZ = XH$ . Since the part of (b) after the displacement of mode 0 preserves photon number, if  $|\alpha, 0\rangle$  is replaced by  $|N, 0\rangle$  at this point in the circuit, the output is the N00N-like state  $e^{-i\pi/4}(|N, 0\rangle + i|0, N\rangle)/\sqrt{2}$ . Equivalently, (c) takes input  $|0\rangle^{\otimes N}$  to the cat-like state  $e^{-i\pi/4}(|0\rangle^{\otimes N} + i|1\rangle^{\otimes N})/\sqrt{2}$ . On this input, the initial  $Z$ s can be omitted, and the final  $X$ s only produce an overall phase, so they, too, can be omitted.

## VI. CONCLUSION

After all this discussion of protocols for phase estimation, what can we say about the prospects for implementing Heisenberg-limited phase estimation in the lab? Probably the best place to try is at microwave frequencies in a qubit/cavity setting, where coherent states can be manipulated relatively easily and where appropriate controlled operations are already available. One might think about performing one of the two-mode coherent-state protocols of Sec. VB. The qubit-

assisted protocol of Fig. 20 requires a controlled swap of the two modes, and the 0BB0-preparing protocols of Figs. 21 and 22(a) require 50/50 beamsplitters and a measurement of parity. These are tall orders, except the parity measurement, which can be done, for example, by mapping to an ancillary qubit as in Fig. 6(c).

If one’s primary goal, however, is Heisenberg-limited phase estimation—and not making 0BB0 states—there is little reason to use two microwave modes. Almost certainly the most practical protocols are the single-mode coherent-state-superposition protocols of Sec. V A. One can imagine implementing the qubit-assisted, single-mode phase-estimation circuit of Fig. 16, with the quantum switches replaced by controlled parities, or perhaps the corresponding modal-cat-state protocols of Fig. 19, with the quantum switches again removed in favor of controlled parities and the final parity measurement performed using an ancillary qubit.

Despite the title of this paper, what we deal with here is not so much interferometry as general phase estimation in interferometric and other settings. Generally, we think about the phase shift as being applied to atoms, as in Ramsey interferometry, or to modes of the electromagnetic field, as in optical interferometry.

In a conventional, quantum-noise-limited interferometer, there is a  $\pi/2$  pulse or beamsplitter immediately before and immediately after the application of the phase shift. Before the initial beamsplitter, there is some relatively simple state preparation, and after the final beamsplitter, there is a relatively simple measurement. Once we generalize to Heisenberg-limited phase estimation, however, we outgrow these beamsplitters. We must consider any preparation procedure before the phase shifter and any measurement procedure after it. In this more general setting, it is clearly better to use a representation that is not tied to the two beamsplitters and that can represent whatever goes on before and after the phase shifter.

This is the reason that quantum circuits provide a far more useful way of representing general protocols for phase estimation and interferometry. Quantum circuits provide a platform-independent pictorial representation of all phase-estimation protocols, allowing us to switch easily from qubits to modes and to visualize—almost to experience, so tactile are the circuit diagrams—the equivalences between different sorts of interferometers and other phase-estimation protocols. The goal of this paper has been to develop tools for manipulating the quantum circuits for phase estimation efficiently.

### Acknowledgments

This article is dedicated to the memory of Krzysztof Wódkiewicz, friend, colleague, and New Mexican. During the time CMC has been at the University of New Mexico, since 1992, Krzysztof spent every other year in Albuquerque. He was an exemplar of excellence, taste, rigor, style, and vitality in doing theoretical physics, both in his teaching and in his research. CMC will always remember him by the way he reappeared in August on his return to UNM after a year in Warsaw: he would bounce down the hallway and burst into the office, eager to share his latest research, always with the same infectious enthusiasm. He approached his work in physics with a vitality that never faltered, and *that* is perhaps the best of several reasons that we will always remember him as a model of a theoretical physicist.

CMC thanks the School of Physical Sciences of the University of Queensland for hospitality when this work was getting started. This work was supported in part by the U.S. Office of Naval Research (Grant No. N00014-07-1-0304). Quantum circuits in this paper were drawn using a modified version of B. Eastin and S. T. Flammia’s Qcircuit package, which draws circuits in

LaTeX; the modified version, provisionally called Qcircuitw, is available from the authors.

- 
- [1] H.-A. Bachor and T. C. Ralph, *A Guide to Experiments in Quantum Optics* (Wiley, New York, 2004).
  - [2] J. J. Bollinger, Wayne M. Itano, D. J. Wineland, and D. J. Heinzen, “Optimal frequency measurements with maximally correlated states,” *Phys. Rev. A* **54**, R4649–R4652 (1996).
  - [3] S. F. Huelga, C. Macchiavello, T. Pellizzari, A. K. Ekert, M. B. Plenio, and J. I. Cirac, “On the improvement of frequency standards with quantum entanglement,” *Phys. Rev. Lett.* **79**, 3865–3868, (1997).
  - [4] A. Shaji and C. M. Caves, “Qubit metrology and decoherence,” *Phys. Rev. A* **76**, 032111 (2007).
  - [5] C. C. Gerry, “Heisenberg-limit interferometry with four-wave mixers operating in a nonlinear regime,” *Phys. Rev. A* **61**, 043811 (2000).
  - [6] A. N. Boto, P. Kok, D. S. Abrams, S. L. Braunstein, C. P. Williams, and J. P. Dowling, “Quantum interferometric optical lithography: Exploiting entanglement to beat the diffraction limit,” *Phys. Rev. Lett.* **85**, 2733–2736 (2000).
  - [7] C. C. Gerry and R. A. Campos, “Generation of maximally entangled photonic states with a quantum-optical Fredkin gate,” *Phys. Rev. A* **64**, 063814 (2001).
  - [8] H. Lee, P. Kok, and J. P. Dowling, “A quantum Rosetta stone for interferometry,” *J. Mod. Opt.* **49**, 2325–2338 (2002).
  - [9] C. C. Gerry, A. Benmoussa, and R. A. Campos, “Nonlinear interferometer as a resource for maximally entangled photonic states: Application to interferometry,” *Phys. Rev. A* **66**, 013804 (2002).
  - [10] R. A. Campos, C. C. Gerry, and A. Benmoussa, “Optical interferometry at the Heisenberg limit with twin Fock states and parity measurements,” *Phys. Rev. A* **68**, 023810 (2003).
  - [11] C. C. Gerry, A. Benmoussa, and R. A. Campos, “Parity measurements, Heisenberg-limited phase estimation, and beyond,” *J. Mod. Opt.* **54**, 2177–2184 (2007).
  - [12] J. P. Dowling, “Quantum optical metrology—the lowdown on high-N00N states,” *Contemp. Phys.* **49**, 125–143 (2008).
  - [13] V. Giovannetti, S. Lloyd, and L. Maccone, “Quantum metrology,” *Phys. Rev. Lett.* **96**, 041401 (2006).
  - [14] S. Boixo, S. T. Flammia, C. M. Caves, and JM Geremia, “Generalized limits for single-parameter quantum estimation,” *Phys. Rev. Lett.* **98**, 090401 (2007).
  - [15] S. Boixo, A. Datta, M. J. Davis, A. Shaji, A. B. Tacla, and C. M. Caves, “Quantum-limited metrology and Bose-Einstein condensates,” *Phys. Rev. A*, to be published, [arXiv:0906.0962 \[quant-ph\]](https://arxiv.org/abs/0906.0962).
  - [16] B. Yurke, Samuel L. McCall, and J. R. Klauder, “SU(2) and SU(1,1) interferometers,” *Phys. Rev. A* **33**, 4033–4054 (1986).
  - [17] R. A. Campos and C. C. Gerry, “Permutation-parity exchange at a beam splitter: Application to Heisenberg-limited interferometry,” *Phys. Rev. A* **72**, 065803 (2005).
  - [18] M. Brune, S. Haroche, J. M. Raimond, L. Davidovich, and N. Zagury, “Manipulation of photons in a cavity by dispersive atom-field coupling: Quantum-nondemolition measurements and generation of ‘Schrödinger cat’ states,” *Phys. Rev. A* **45**, 5193–5214 (1992).
  - [19] L. Davidovich, A. Maali, M. Brune, J. M. Raimond, and S. Haroche, “Quantum switches and nonlocal microwave fields,” *Phys. Rev. Lett.* **71**, 2360–2363, (1993).
  - [20] L. Davidovich, M. Brune, J. M. Raimond, and S. Haroche, “Mesoscopic quantum coherences in cavity QED: Preparation and decoherence monitoring schemes,” *Phys. Rev. A* **53**, 1295–1309 (1996).
  - [21] L. G. Lutterbach and L. Davidovich, “Method for direct measurement of the Wigner function in cavity QED and ion traps,” *Phys. Rev. Lett.* **78**, 2547–2550 (1997).
  - [22] L. G. Lutterbach and L. Davidovich, “Non-classical states of the electromagnetic field in cavity QED,” *Opt. Exp.* **3**, 145–153 (1998).
  - [23] J. M. Raimond, M. Brune, and S. Haroche, “Colloquium: Manipulating quantum entanglement with atoms and photons in a cavity,” *Rev. Mod. Phys.* **73**, 565–581 (2001).
  - [24] L. Davidovich, “Decoherence and quantum-state measurement in quantum optics,” in *Decoherence and Entropy in Complex Systems: Selected Lectures from DICE 2002*, edited by H.-T. Elze (Springer, Berlin, 2004), pages 313–319.
  - [25] K. Wódkiewicz, “Stochastic decoherence of qubits,” *Opt. Exp.* **8**, 145–152 (2001).

- [26] S. Daffer, K. Wódkiewicz, and J. K. McIver, “Quantum Markov channel for qubits,” *Phys. Rev. A* **67**, 062312 (2003).
- [27] S. Daffer, K. Wódkiewicz, and J. K. McIver, “Bloch equations and completely positive maps,” *J. Mod. Opt.* **51**, 1843–1858 (2004).
- [28] S. Daffer, K. Wódkiewicz, J. D. Cresser, and J. K. McIver, “Depolarizing channel as a completely positive map with memory,” *Phys. Rev. A* **70**, 010304(R) (2004).
- [29] A. Dragan and K. Wódkiewicz, “Depolarization channels with zero-bandwidth noises,” *Phys. Rev. A* **71**, 012322 (2005).
- [30] E. Knill, R. Laflamme, and G. J. Milburn “A scheme for efficient quantum computation with linear optics,” *Nature* **409**, 46–52 (2001).
- [31] T. C. Ralph, A. G. White, W. J. Munro, and G. J. Milburn, “Simple scheme for efficient linear optics quantum gates,” *Phys. Rev. A* **65**, 012314 (2002).
- [32] This is because the algebra of the operators  $I$ ,  $J_z$ , and  $J_{\pm} = J_x \pm iJ_y$  spans the space of operators on the space of angular momentum  $J = N/2$ . One way to see this is to notice that any outer product in the angular-momentum basis,  $|J, m\rangle\langle J, m'|$ , is a multiple of  $J_-^{J-m}|J, J\rangle\langle J, J|J_+^{J-m'}$ , which in turn is a multiple of  $J_-^{J-m}J_+^{2J}J_zJ_-^{2J}J_+^{J-m'}$ .
- [33] M. A. Nielsen and I. L. Chuang, *Quantum Computation and Quantum Information* (Cambridge University Press, Cambridge, England, 2000).
- [34] S. Boixo, A. Datta, S. T. Flammia, A. Shaji, E. Bagan, and C. M. Caves, “Quantum-limited metrology with product states,” *Phys. Rev. A* **77**, 012317 (2008).
- [35] M. J. Woolley, G. J. Milburn, and C. M. Caves, “Nonlinear quantum metrology using coupled nanomechanical resonators,” *New J. Phys.* **10**, 125018 (2008).
- [36] S. Boixo, A. Datta, M. J. Davis, S. T. Flammia, A. Shaji, and C. M. Caves, “Quantum metrology: Dynamics vs. entanglement,” *Phys. Rev. Lett.* **101**, 040403 (2008).
- [37] R. B. Griffiths and C.-S. Niu, “Semiclassical Fourier transform for quantum computation, *Phys. Rev. Lett.* **76**, 3228–3231 (1996).
- [38] R. Cleve, A. Ekert, L. Henderson, C. Macchiavello, M. Mosca, “On quantum algorithms,” *Complexity* **4**, 33–42 (1999).
- [39] G. Nogues, A. Rauschenbeutel, S. Osnaghi, P. Bertet, M. Brune, J. M. Raimond, S. Haroche, L. G. Lutterbach, and L. Davidovich, “Measurement of a negative value for the Wigner function of radiation,” *Phys. Rev. A* **62**, 054101 (2000).
- [40] P. Bertet, A. Auffeves, P. Maioli, S. Osnaghi, T. Meunier and M. Brune, J. M. Raimond, and S. Haroche, “Direct measurement of the Wigner function of a one-photon Fock state in a cavity,” *Phys. Rev. Lett.* **89**, 200402 (2002).
- [41] M. O. Scully and K. Drühl, “Quantum eraser: A proposed photon correlation experiment concerning observation and ‘delayed choice’ in quantum mechanics,” *Phys. Rev. A* **25**, 2208–2213 (1983).
- [42] M. O. Scully, B.-G. Englert, and H. Walther, “Quantum optical tests of complementarity,” *Nature* **351**, 111–116 (1991).
- [43] S. P. Walborn, M. O. Terra Cunha, S. Pádua, and C. H. Monken, “Double-slit quantum eraser,” *Phys. Rev. A* **65**, 033818 (2002).
- [44] A. Chiruvelli and H. Lee, “Parity measurements in quantum optical metrology,” [arXiv:0901.4395](https://arxiv.org/abs/0901.4395) [quant-ph].
- [45] Y. Gao, C. F. Wildfeuer, P. M. Anisimov, H. Lee, and J. P. Dowling, “Super-resolution at the shot-noise limit with coherent states and photon-number-resolving detectors,” [arXiv:0907.2382](https://arxiv.org/abs/0907.2382) [quant-ph].
- [46] S. Wallentowitz and W. Vogel, “Unbalanced homodyning for quantum state measurements,” *Phys. Rev. A* **53**, 4528–4533 (1996).
- [47] K. Banaszek and K. Wódkiewicz, “Direct probing of quantum phase space by photon counting,” *Phys. Rev. Lett.* **76**, 4344–4347 (1996).
- [48] K. Banaszek, C. Radzewicz, K. Wódkiewicz, and J. S. Krasieński, “Direct measurement of the Wigner function by photon counting,” *Phys. Rev. A* **60**, 674–677 (1999).
- [49] M. Hofheinz, H. Wang, M. Ansmann, R. C. Bialczak, E. Lucero, M. Neeley, A. D. O’Connell, D. Sank, J. Wenner, J. M. Martinis, and A. N. Cleland, “Synthesizing arbitrary quantum states in a superconducting resonator,” *Nature* **459**, 546–549 (2009).
- [50] C. K. Law and J. H. Eberly, “Arbitrary control of a quantum electromagnetic field,” *Phys. Rev. Lett.* **76**, 1055–1058 (1996).

- [51] M. Brune, E. Hagley, J. Dreyer, X. Maître, A. Maali, C. Wunderlich, J. M. Raimond, and S. Haroche, “Observing the progressive decoherence of the ‘meter’ in a quantum measurement,” *Phys. Rev. Lett.* **77**, 4887–4890 (1996).
- [52] C. Guerlin, J. Bernu, S. Deléglise, C. Sayrin, S. Gleyzes, S. Kuhr, M. Brune, J.-M. Raimond, and S. Haroche, “Progressive field-state collapse and quantum non-demolition photon counting,” *Nature* **448**, 889–893 (2007).
- [53] M. Brune, J. Bernu, C. Guerlin, S. Deléglise, C. Sayrin, S. Gleyzes, S. Kuhr, I. Dotsenko, J.-M. Raimond, and S. Haroche, “Process tomography of field damping and measurement of Fock state lifetime by quantum nondemolition photon counting in a cavity,” *Phys. Rev. Lett.* **101**, 240402 (2008).
- [54] S. Gleyzes, S. Kuhr, C. Guerlin, J. Bernu, S. Deléglise, U. B. Hoff, M. Brune, J.-M. Raimond, and S. Haroche, “Quantum jumps of light recording the birth and death of a photon in a cavity,” *Nature* **446**, 297–300 (2007).
- [55] S. Deléglise, I. Dotsenko, C. Sayrin, J. Bernu, M. Brune, J.-M. Raimond, and S. Haroche, “Reconstruction of non-classical cavity field states with snapshots of their decoherence,” *Nature* **455**, 510–514 (2008).
- [56] F. Toscano, D. A. R. Dalvit, L. Davidovich, and W. H. Zurek, “Sub-Planck phase-space structures and Heisenberg-limited measurements,” *Phys. Rev. A* **73**, 023803 (2006).
- [57] B. Yurke and D. Stoler, “Generating quantum mechanical superpositions of macroscopically distinguishable states via amplitude dispersion,” *Phys. Rev. A* **57**, 13–16 (1986).
- [58] R. Tanaś and S. Kielich, “Role of the higher optical Kerr nonlinearities in self-squeezing of light,” *Quant. Opt.* **2**, 23–33 (1990). *Quantum Optics: Journal of the European Optical Society B* has gone through a series of name changes and mergers and can now be found at IOP Publishing as part of *Journal of Physics B: Atomic, Molecular and Optical Physics*.
- [59] A. Miranowicz, R. Tanaś, and S. Kielich, “Generation of discrete superpositions of coherent states in the anharmonic oscillator model,” *Quant. Opt.* **2**, 253–265 (1990). See note on journal *Quantum Optics* in Ref. [58].
- [60] C. C. Gerry, “Generation of optical macroscopic quantum superposition states via state reduction with a Mach-Zender interferometer containing a Kerr medium,” *Phys. Rev. A* **59**, 4095–4098 (1999).
- [61] C. C. Gerry and R. Grobe, “Nonlocal entanglement of coherent states, complementarity, and quantum erasure,” *Phys. Rev. A* **75**, 034303 (2007).
- [62] D. A. R. Dalvit, R. L. de Matos Filho, and F. Toscano, “Quantum metrology at the Heisenberg limit with ion trap motional compass states,” *New J. Phys.* **8**, 276 (2006).
- [63] W. H. Zurek, “Sub-Planck structure in phase space and its relevance for quantum decoherence,” *Nature* **412**, 712–717 (2001).
- [64] S. Schneider, H. M. Wiseman, W. J. Munro, and G. J. Milburn, “Measurement and state preparation via ion trap quantum computing,” *Fortschritte Phys.* **46**, 391–400 (1998).
- [65] We studiously avoid the N00N-state ordering for 0BB0 states.
- [66] A. Datta, V. Madhok, A. Shaji, A. B. Tacla, and C. M. Caves, “Heisenberg-limited phase estimation with mode-entangled coherent states,” in preparation.
- [67] C. C. Gerry and R. A. Campos, “Generation of maximally entangled states of a Bose-Einstein condensate and Heisenberg-limited phase resolution”, *Phys. Rev. A* **68**, 025602 (2003).